Earth-Science Reviews 232 (2022) 104109

Contents lists available at ScienceDirect

Earth-Science Reviews

journal homepage: www.elsevier.com/locate/earscirev

Dynamic continuous hydrocarbon accumulation (DCHA): Existing theories and a new unified accumulation model

Tao Hu [a,b], Xiongqi Pang [a,b,*], Fujie Jiang [a,b,*], Chenxi Zhang [a,b], Guanyun Wu [a,b], Meiling Hu [a,b], Lin Jiang [c], Qifeng Wang [c], Tianwu Xu [d], Yao Hu [a,b], Shu Jiang [e], Wenyang Wang [f], Maowen Li [g]

[a] State Key Laboratory of Petroleum Resources and Prospecting, Beijing 102249, China
[b] College of Geosciences, China University of Petroleum (Beijing), Beijing 102249, China
[c] Research Institute of Petroleum Exploration and Development, PetroChina, Beijing 100083, China
[d] Research Institute of Exploration and Development, Zhongyuan Oilfield Company, SINOPEC, Puyang 457001, China
[e] Energy & Geoscience Institute, University of Utah, Salt Lake City, UT 84108, USA
[f] State Key Laboratory of Lithospheric Evolution, Institute of Geology and Geophysics, Chinese Academy of Sciences, Beijing 100029, China
[g] State Key Laboratory of Shale Oil and Shale Gas Resources and Effective Development, Sinopec Petroleum Exploration and Production Research Institute, Beijing 100083, China

ARTICLE INFO

Keywords:
Dynamic continuous hydrocarbon accumulation
Accumulation model
Petroleum geology theory
Petroleum source
Charging times
Charging force
Dongpu Depression

ABSTRACT

Replacing coal with cleaner hydrocarbon resources is a viable solution to reach carbon neutrality goals over time, especially given the current lack of growth in green energy resources (e.g., hydro, solar, wind, geothermal) globally. Hydrocarbon resources offer a low-carbon, low-waste, large-scale, rapid solution. Dynamic continuous hydrocarbon accumulation (DCHA) exists widely in sandstone and shale reservoirs and has enormous resource potential. However, understanding the accumulation mechanisms and models of DCHAs in different structural locations is highly challenging. In this study, we first extensively review hydrocarbon resources derived from hydrocarbon accumulation and identify key scientific issues and theories. We then take the well-known typical DCHA in the Bohai Bay Basin in eastern China as a case, and combine multiple analytical methods, such as biomarker analysis, petroleum and aqueous inclusion analysis, quantitative fluorescence analysis, microscopic thin section observations, and basin modeling, to investigate petroleum sources, charging times, and charging forces. The results of our study show that the DCHA is a superimposed accumulation of multiple petroleum reservoir types with multiple petroleum sources, charging times, charging forces, and modes. Petroleum reservoirs at high structural locations are conventional trap reservoirs accumulated by buoyancy in the early stage, with long migration distances. Petroleum reservoirs at the sag location are deep unconventional petroleum reservoirs accumulated by the petroleum generation pressurization force in the middle stage, with short migration distances. Petroleum reservoirs at the slope location are superpositions of conventional traps and deep unconventional petroleum reservoirs in the middle and late stages, with moderate migration distances.

1. Introduction

Petroleum is the most important primary energy source on Earth. Its proportion in the global primary energy supply is expected to remain at >50% by 2040 (EIA, 2019; Exxon, 2018). The world's carbon emissions are set to peak in the next few decades. To achieve China's carbon peak and carbon neutrality goals by 2030 and 2060, respectively (Liu, 2015b; Zhang et al., 2021), replacing coal with hydrocarbons as soon as possible to replenish weak growth in clean energy is one of the most viable approaches. However, this approach requires further strengthening of petroleum exploration and development.

Since the world's first industrial oil well was successfully drilled in 1859 (Jia, 2017), the global petroleum industry has experienced >160 years of development. During this period, corresponding to three significant petroleum exploration discoveries, three important petroleum geological theories were established. White (1885) proposed the "Anticlinal Theory for Petroleum Accumulation" which stated that buoyancy is the driving force for petroleum accumulation, and oil, gas and water are differentiated according to their densities. Low-density oil and gas occupy the top of the anticline, while high-density water is at the

* Corresponding authors at: State Key Laboratory of Petroleum Resources and Prospecting, Beijing 102249, China.
E-mail addresses: pangxq@cup.edu.cn (X. Pang), jfjhtb@163.com (F. Jiang).

https://doi.org/10.1016/j.earscirev.2022.104109
Received 12 October 2021; Received in revised form 27 June 2022; Accepted 3 July 2022
Available online 8 July 2022

bottom. Therefore, the top of the anticline is considered to be the best area for petroleum exploration. Guided by this theory, a large number of anticlinal hydrocarbon resources have been discovered. Mccollough (1934) discovered that petroleum accumulation requires traps, including reservoirs, caprocks and blocking conditions, which have uniform oil, gas and water interfaces and proposed the "Trap Theory for Petroleum Accumulation". Guided by this theory, a large number of lithologic, stratigraphic and fault petroleum reservoirs located in structural slopes have been discovered. More recently, "Continuous Petroleum Accumulation Theory" (Schmoker, 1995) and "Unconventional Petroleum Theory" (Law and Curtis, 2002a) have promoted the large-scale discovery of tight and shale petroleum reservoirs, respectively.

Dynamic continuous hydrocarbon accumulation (DCHA) refers to extensive petroleum accumulation in both sandstone and shale reservoirs, which is a dynamic process that exists continuously in different structural locations (highs, slopes, and sags) within a single layer or multiple layers in a petroliferous basin (Schmoker, 1995; Li et al., 2017; Pang et al., 2014b). In addition to the petroleum accumulated in unconventional tight reservoirs, DCHAs include genetically related petroleum accumulated in conventional reservoirs. DCHAs exist in large areas with no obvious oil-gas-water interface boundaries (Zou et al., 2013, 2019), and have unusual mechanisms for petroleum accumulation and interstitial flow (Etherington and McDonald, 2004; Guo et al., 2017; Law and Curtis, 2002b; Rose, 1981; Spencer and Mast, 1986).

Global petroleum exploration practices have shown that DCHAs widely exist in deep strata adjacent to source rocks in petroliferous basins and have great resource potential (Brown et al., 1982; Zhang et al., 2015; Zhao, 2012; Zou et al., 2013, 2015; Craig et al., 2018; Cao et al., 2020; Li et al., 2021) (Fig. 1). Studies on the genetic mechanisms and distribution of individual DCHA reservoirs (Jin and Zhang, 1999; Law and Curtis, 2002a; Zhang, 2003; Zhang et al., 2003) have achieved considerable progress. They include conventional anticline (high structural locations), lithological-stratigraphic and fault (structural slopes and high locations), and tight (structural slopes and sag locations) petroleum reservoirs (Ayers Jr, 2002; Law and Curtis, 2002b; Montgomery et al., 2002; Schmoker, 2002). However, these separate studies on individual DCHA reservoirs have failed to systematically uncover intrinsic and substantial relationships among different types of petroleum reservoirs in different structural locations, resulting in a lack of systematic and coherent understandings of some key issues in petroleum geology theory. For example, **the petroleum properties in DCHAs in different structural locations show clear progressive changes.** Specifically, as the structural locations change from high to slope to sag, 1) the petroleum phases change from heavy oil to light oil, to condensate oil, and finally to dry gas, 2) the oil-gas-water interfaces change from a normal interface (gas at the top, oil at the middle, and water at the bottom) to an inverted oil-water interface (water at the top and oil at the bottom) to an inverted oil-gas interface (oil at the top and gas at the bottom) and finally to no gas-water interface (gas and water completely mixed), 3) the density and viscosity of oil decrease gradually, and 4), the gas-oil ratio (GOR) and thermal maturity increase gradually. This phenomenon is common in the Bohai Bay Basin (Cheng et al., 2015; Hu, 2019; Jin and Zhang, 1999; Zhang, 2003), Songliao Basin (Wu et al., 2007), Sichuan Basin (Wu et al., 2007), Ordos Basin (Zhao, 2012; Zhao et al., 2013; Zhao et al., 2016; Zou et al., 2013), Tuha Basin (Zhang et al., 2003), Junggar Basin (Hu et al., 2018; Zhi et al., 2021), and Tarim Basin (Pang et al., 2014b) in China, the Chu-Salesu Basin (Pang et al., 2014b) in Kazakhstan, and the Fort Worth Basin (Pollastro, 2007) and San Joaquin Valley (Larue et al., 2018) in the USA. **Studies on the accumulation process for different types of petroleum reservoirs in DCHAs in different structural locations are derived only from hypotheses about geological phenomena and are subjective.** Specifically, understandings of DCHAs formed by superimposition with different types of petroleum reservoirs accumulated in different periods are mainly based on the characteristics of basin tectonic evolution and

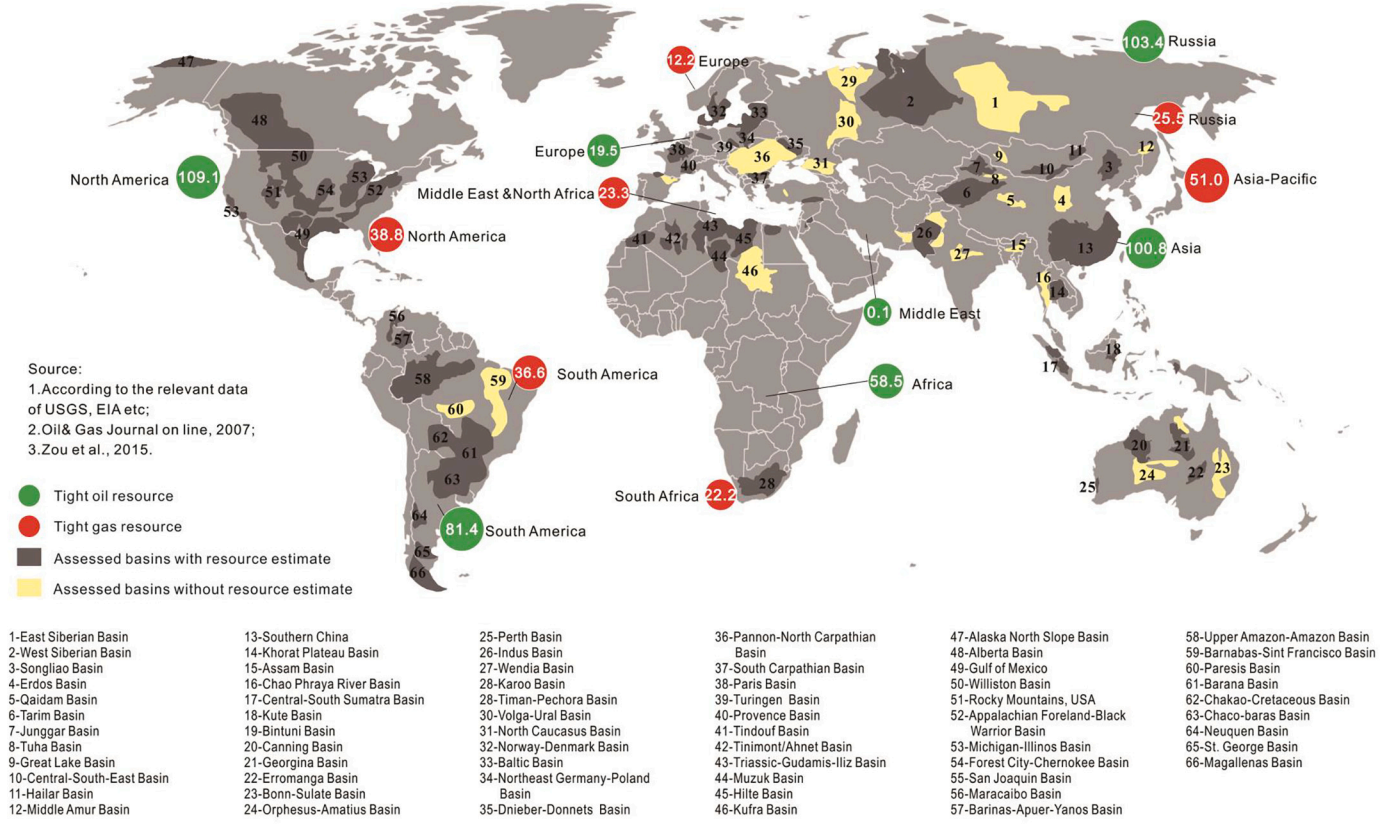

Fig. 1. Global tight sandstone oil and gas resources.

source rock-reservoir assemblages, but little effort has been made to clarify the accumulation history of DCHAs (Guo, 2014; Jiang et al., 2006; Pang et al., 2014b; Pang et al., 2021; Pang et al., 2014b; Pang et al., 2000; Pang et al., 2021a; Schenk, 2005; Tao et al., 2011; Yang et al., 2022; Zhang et al., 2003).

In the Dongpu Depression, Bohai Bay Basin, China, Paleogene petroleum exploration from anticline, lithological, stratigraphic, and fault hydrocarbon reservoirs in high structural locations has entered a highly mature stage (Duan et al., 2008), and the remaining exploration has gradually advanced to the structural slope and sag locations. Commercial oil and gas flows have been obtained from many wells targeting Paleogene tight sandstone reservoirs on the slope and sag. Furthermore, statistical oil test data of exploratory wells near the sag show that almost all wells drilled in the tight sandstone reservoirs have noticeable oil and gas shows although oil and gas yields are generally low, and commercial wells are limited. This fact indicates that the abundance of oil and gas in the slope and sag is low, but the distribution area is large. As the structural location deepens from high to slope to sag, the petroleum phase, oil-gas-water interface, density, viscosity, and GOR show clear continuous changes. The petroleum accumulated in the Paleogene Shahejie Formation of the Dongpu Depression is distributed from deep to shallow and from bottom to top and shows the basic geological characteristics of a DCHA. As a well explored area, the Dongpu Depression, especially the Shahejie Formation, together with its huge exploration data, provides a good opportunity for addressing issues related to the genetic mechanism and distribution patterns of DCHAs, including the intrinsic relationships among different types of petroleum reservoirs in DCHAs in different structural locations, progressive accumulation processes, and accumulation models.

In this study, we first reviewed DCHA theories, and highlighted key scientific issues that need to be solved. Then we considered a typical DCHA in the Dongpu Depression as a case study and used analytical data acquired from oil, shale and sandstone drill samples, such as biomarker analysis, petroleum and aqueous inclusion analysis (petrographic and homogenization temperature), quantitative fluorescence analysis, and microscopic thin section observations, to determine the oil sources, charging times, charging forces, and basin modeling for the DCHA at different structural locations. Finally, the above studies were combined with the structural and depositional settings to reconstruct the charging history and establish a new unified accumulation model for DCHA exploration.

2. Review of DCHA theories

2.1. Early period: 1910s - 1990

DCHAs were noted in early studies; for example, such as the large amounts of natural gas in the Niobrara Formation when the Goodland No. 1 Well in eastern Colorado, US was drilled in 1912 (Brown et al., 1982), the Rabachi Gas Field was identified in the Green River Basin in 1924 and the Cretaceous Blanco Gas Field was identified in the San Juan Basin in 1927. Limited by the technology of the time, this type of natural gas was not economically exploited. Due to limited knowledge of its geological characteristics and accumulation, this natural gas was referred to as “subtle gas” (Zhang et al., 2007).

Wilson (1934) classified petroleum reservoirs into “closed” and “open” reservoirs, and defined the former as having clear trap boundaries, including structures, faults, lithology, and stratigraphic petroleum reservoirs, and the latter as having no clear trap boundaries, such as tight sandstone gas reservoirs. Therefore, Wilson successfully foresaw the existence of “open petroleum reservoirs” at that time and classified them into a single category, but he deemed that they had no industrial value for the time being (Wilson, 1934). Cretaceous tight sandstone gas reservoirs in the San Juan Basin began to be developed in the early 1950s. Silver found that these reservoirs lacked edge water and bottom water and contained extensive gas (Jin et al., 1997). Hydraulic fracturing experiments conducted in the USA from the late 1960s to the early 1970s were also based on the assumption that strata are extensively gas-bearing (Law and Curtis, 2002a). In 1974, foam fracturing technology was first successfully applied to the exploitation of the Niobrara tight gas reservoir, confirming the existence of large natural gas resources in tight reservoirs (Brown et al., 1982).

The Elmworth giant tight sandstone gas field was discovered in the Alberta Basin in western Canada in 1976. By analyzing the distribution characteristics of the Elmworth, Milk River, and Blanco Gas Fields in North America in 1979, Masters (1979) found that gas in tight sandstone gas reservoirs was mostly distributed in the central or deeper parts of basins, such as “deep basin gas”, and held that such basins have an obvious regional inverted gas-water interface. The relative permeability changes in gas and water provide obstacles for deep basin gas accumulation and, when the water saturation is $\geq$60%, the gas in the tight sandstone reservoir is almost completely blocked, forming a water blockage seal (Masters, 1979). Leythaeuser et al. (1980), Welte et al. (1984) and Gies (1984) later analyzed the geological and geochemical data of deep basin gas in the Alberta Basin and proposed the concept of a “dynamic trap” in which plugging conditions are not required; thus, gas migrates slowly in tight sandstone reservoirs (Silin et al., 1984). Continued gas diffusion leads to a continuous gas supply, which enables deep basin gas reservoirs to remain in a dynamic equilibrium state. Gies (1984) pointed out that gas migration in deep basin gas reservoirs is not controlled by buoyancy. Based on formation pressure analysis of the Cadomin Formation in the Alberta Basin, Gies (1984) conducted experiments on abnormal formation pressures in deep basin gas reservoirs and further found that such reservoirs show abnormally low formation pressures. Cant (1983, 1986) believed that the inverse gas-water interface in deep basin gas reservoirs is mainly due to rock diagenesis, which is termed a “bottleneck trap” (Masters, 1984). Because the concept of deep basin gas is not based on the origin or migration mechanism, it is often confused with other concepts such as “deep strata gas” and “deep source gas”. The mechanism cannot be distinguished from the hydrodynamics, lithology and tight sandstone gas reservoirs (the accumulation process is unclear). Therefore, the deep basin gas concept is no longer frequently used.

Walls (1982) and Spencer and Mast (1986) conducted studied gas reservoirs in the Spirit River Basin in Western Alberta and the Cotton Valley Basin in Eastern Texas and proposed the concept of “tight sandstone gas”. However, this concept does not consider the gas accumulation mechanism and thus cannot provide effective guidance for tight sandstone gas exploration. In fact, the term tight sandstone gas comes from customary usage, which already includes the meaning of deep basin gas reservoirs (Law and Curtis, 2002b). Law and Dickinson (1985) and Spencer (1987) studied the Great Green River Basin in the USA and proposed that thermal generation and gas accumulation in tight sandstone reservoirs induce abnormally high pressures during the formation of tight sandstone gas. Law and Dickinson (1985) proposed a conversion model of abnormal formation pressure and suggested that abnormal formation pressure is related to the gas charging rate and gas loss rate, and that tectonic uplift and sedimentary strata denudation can also cause formation pressure changes from high to low.

Rose (1981) proposed “basin-centered gas accumulation” when studying tight sandstone gas reservoirs in the Roton Basin, southern Colorado, and indicated that there is no edge water or bottom water in this type of accumulation. Berkenpas (1991) analyzed the accumulation process of deep basin gas/basin-centered gas accumulation and proposed a dynamic balance among buoyancy, interfacial tension, and differential pressure for its formation. Therefore, Berkenpas (1991) suggested that the key factors controlling deep basin gas accumulation are the strata dip and pore throat radius. Xu (1991) analyzed the geological characteristics of tight sandstone gas reservoirs in the Dongpu Depression, Bohai Bay Basin, China, and found that tight sandstone gas is distributed in the slope and sag, with porosities and permeabilities of $<$12% and 1 mD, respectively. Law and Spencer (1993)conducted

research on the reservoir characteristics, gas sources and resource potential of tight sandstone gas reservoirs. The dual sealing effect of capillary pressure and abnormal pressure has been suggested to promote the formation of deep basin gas/basin-centered gas accumulation (Surdam et al., 1995, 1996). At this stage, tight sandstone petroleum reservoirs were referred to as unconventional petroleum resources that could not be economically produced without massive production increase measures or special exploitation methods (Etherington and McDonald, 2004). However, this concept is based on human understanding and the development of appropriate techniques and cannot objectively reflect the geological characteristics and reservoir formation mechanisms of tight sandstone reservoirs.

2.2. Middle period: 1990s - 2010

Schmoker (1995) proposed the concept of "continuous petroleum accumulation", which has a wide distribution of hydrocarbons, fuzzy oil-gas boundaries, low media permeability, and abnormal pressures, lacks traps and caprocks, and is in close contact with source rocks and reservoirs; in addition, its buoyancy does not play a key role in hydrocarbon migration. Continuous petroleum accumulation refers to continuous natural gas, including deep basin gas, basin-centered gas accumulation, tight sandstone gas, shale gas, coalbed gas, shallow sandstone biogas, and natural gas hydrate. Asakawa (1995) reviewed the current status of unconventional gas exploration and development in the USA, superimposed the horizontal distribution of tight sandstone gas, coalbed gas, shale gas, and water-soluble gas and discovered that shale gas, coalbed gas and tight sandstone gas often develop in the same basin. He speculated that there may be some correlation among them. Tyler et al. (1995) described the San Juan Basin as a basin with multiple types of gas reservoirs after studying the occurrence characteristics of coalbed gas resources. Based on the data sourced from Masters (1979, 1984), Jin and Zhang (2003) compiled a cross-sectional map of various types of gas reservoirs in the Alberta Basin and found that the coalbed gas reservoirs, deep basin gas / basin-centered gas accumulation reservoirs and conventional gas reservoirs are distributed in order (Zhang et al., 2003).

Jin and Zhang (1999) analyzed the accumulation process of deep basin gas/basin-centered gas accumulation from the perspective of dynamics and held that the "capillary pressure seal" is the key feature of its formation. Pang et al. (2000) analyzed deep basin gas/basin-centered gas accumulation and proposed that its key characteristics are tight reservoirs, the interlinkage of source rocks and reservoirs, and the integration of reservoirs and caprocks. Moreover, Pang et al. (2000) studied the accumulation dynamics of deep basin gas/basin-centered gas accumulation and held that the formation of deep basin gas depends on four dynamic forces: hydrostatic pressure, capillary resistance, buoyancy, and gas thermal expansion. Specifically, petroleum first enters tight reservoirs as a result of the gas expansion force, and then, due to less buoyancy than capillary force, petroleum cannot continue to migrate upward, which promotes deep basin gas/basin-centered gas accumulation formation. To further investigate the accumulation mechanism of deep basin gas/basin centered gas accumulation, Zhang (2001) proposed the concept of a "progressive sequence for hydrocarbon accumulation" to characterize a series of petroleum reservoirs with genetic correlations and accumulation mechanism transitions. However, the characterization was derived from basin tectonic evolution and source rock-reservoir assemblage, and no actual data are available to support this view. Law and Curtis (2002b) pointed out that all basins in the United States contain basin centered gas accumulation. Most basins in China are characterized by rich gas sources and tight reservoirs; thus, basin-centered gas accumulation resources should be abundant in China (Wang, 2000). Pang et al. (2003) studied critical conditions for the formation of deep basin gas/basin-centered gas accumulation through physical simulation experiments and held that they are controlled by "force balance" and "material balance". "Force balance" refers to the lower limit of buoyancy accumulation in petroliferous basins (Pang et al., 2021), which can be expressed by the critical porosity, permeability, and pore throat radius values of sandstone reservoirs, which are 12%, 1 mD and 1 μm, respectively (Pang et al., 2014b). Only when sandstone reservoirs reach "force balance" can they form the "water seal condition", which controls the maximum distribution range of deep basin gas/basin-centered gas accumulation. "Material balance" controls the actual range of deep basin gas/basin-centered gas accumulation, and when the natural gas supply is greater than the loss, the range continues to expand. Otherwise, deep basin gas/basin centered gas accumulation cannot be formed or gradually shrinks (Pang et al., 2003). Starting from basic conditions for the formation of deep basin gas/basin centered gas accumulation (adjacent to source rocks), Zhang et al. (2003) suggested using "source-contacting gas" instead of "deep basin gas" and summarized the basic characteristics: 1) no edge water and bottom water; 2) piston mode of petroleum accumulation, in which pore water is propelled by natural gas injected from the bottom, and the two move synchronously in tight and homogeneous reservoirs, acting like a piston (Jin and Zhang, 2003; Zhang et al., 2008); 3) tight sandstone reservoir, sufficient gas source, interlinked source rock and reservoir and integrated reservoir and caprock; 4) hydrocarbon generation expansion force as the key accumulation power; and 5) continuous transitions in both mechanism and distribution with conventional gas reservoirs.

2.3. Contemporary period: 2011 – Present day

As the depth of exploration has increased, petroleum geologists have noticed that many oil and gas reservoirs are located near sags or even in sag centers. Therefore, Zhao et al. (2004) proposed the concept of "sag-wide oil-bearing" reservoirs in oil-rich depressions, but at that time, most scholars regarded these reservoirs located in the lower parts of the depressions as lithologic oil and gas reservoirs. Schenk (2005) extended the geological characteristics of continuous gas accumulation to continuous oil accumulation and summarized 16 geological characteristics. According to the sequential order between hydrocarbon generation and expulsion periods and tight periods of reservoirs, Jiang et al. (2006) classified tight sandstone reservoirs as "accumulation first" and "accumulation later". The former is a type of deep basin gas/basin-centered gas accumulation that is distributed in the sag center or slope. The latter is a trap that formed first and is dense and distributed in high structural high locations. This study distinguishes two types of tight sandstone gas reservoirs with distinct reservoir-forming mechanisms, but it explains only the formation process of tight oil and gas from a geological perspective. Wu et al. (2007) discovered a large area of continuous sandstone oil reservoirs in the Fuyang Formation at the syncline of the Sanzhao Sag, Songliao Basin and termed it a "syncline oil reservoir". He held that the retention effect is the key to its accumulation. Ma (2008) subsequently studied the dynamic mechanism and development model of this reservoir and confirmed the existence of a lower limit of buoyancy accumulation.

With the further exploration of lithologic and stratigraphic petroleum reservoirs, geologists discovered large-scale contiguous petroleum reservoirs in the center of the Ordos Basin. Therefore, Zou et al. (2009a, 2009b) introduced the concept of continuous petroleum reservoirs into China and elaborated the formation conditions and distribution characteristics. In response to of the question of "whether petroleum accumulates before or after reservoir densification", global scholars have conducted many physical and numerical simulation experiments and reached two consensuses: 1) petroleum can enter tight reservoirs driven by overpressure, indicating the existence of the geological process of "accumulation after reservoir densification"; and 2) reservoirs can become tight by compaction and diagenesis after petroleum charging, indicating the existence of the geological process of "accumulation before reservoir densification" (Abbad, 2012; Dmitriy et al., 2011; Guo et al., 2013; Khalili et al., 2012; Mehmani et al., 2011; Rahmanian et al., 2011). Tao et al. (2011) analyzed the "external to the source rock" type

of continuous petroleum reservoirs (tight sandstone or tight limestone) from the perspectives of "genesis" and "distribution" and held that its continuity is in terms of its "genesis". Thereafter, the accumulation characteristics were summarized as piston charging and continuous accumulation. Pang et al. (2012) systematically expounded the controlling effect of fluid dynamic fields on hydrocarbon migration and accumulation in petroliferous basins. Zhao (2012) divided unconventional hydrocarbons into three types: continuous (coalbed gas and shale gas), quasi-continuous (tight oil and gas), and discontinuous (most oil sands, heavy oil and super heavy oil). Soon afterward, Zhao et al. (2013) proposed continuous, quasi-continuous, and discontinuous accumulation models and held that deep basin gas/basin centered gas accumulation and conventional petroleum reservoirs represent two end members of the reservoir sequence. The quasi-continuous petroleum reservoir is a transitional tight hydrocarbon accumulation, and its geological characteristics include the following: 1) it is composed of several small- and medium-scale petroleum reservoirs adjacent to each other, and the oil and gas are quasi-continuous distributions. The oil, gas and water distributions are complex, and there is no obvious inverted oil-gas-water interface. 2) Petroleum charging is dominated by large-area diffuse vertical displacement, with direct primary migration or short-distance secondary accumulation. 3) Petroleum accumulation occurs before reservoir densification or at the same time, with strong heterogeneity. Zou et al. (2013) summarized the characteristics of continuous tight sandstone petroleum reservoirs, including the coexistence of source rocks and reservoirs, low porosity and permeability, extensive nanopores, extensive and continuous distribution of oil and gas reservoirs, no obvious traps, weak buoyancy and hydrodynamic forces, seepage flows that do not obey Darcy's Law, poor phase difference, no uniform oil-gas-water interface and pressure system, and variable oil-gas saturation. Guo (2013) verified the existence of a lower limit of buoyancy-driven hydrocarbon accumulation by physical simulation experiments and confirmed that the critical porosity threshold is approximately 10% through numerical simulation.

Pang et al. (2014a, 2014b) studied the formation mechanism, development model, and predicted distribution of continuous petroleum reservoirs and proposed the concept of "superimposed continuous petroleum reservoirs". Superimposed continuous petroleum reservoirs refers to unconventional petroleum reservoirs that are widely distributed in petroliferous basins, appear continuously in patches and zones, and are not controlled by buoyancy. According to the different geological characteristics and accumulation mechanisms, superimposed continuous petroleum reservoirs can be subdivided into conventional tight petroleum reservoirs, deep basin tight petroleum reservoirs and composite tight petroleum reservoirs, with the following characteristics: 1) tight and petroleum-rich reservoirs in both high and low structural locations; 2) large petroleum-bearing areas and variable yields; 3) development of multi-interval layers in the vertical source rock series with both high and low pressures; and 4) abundant resources with complex relationships between oil, gas and water distributions (Pang et al., 2014b; Pang et al., 2014b). Guo (2014) revealed the near-source accumulation mechanism of continuous tight sandstone gas reservoirs. Cheng et al. (2015) studied petroleum reservoirs in the upper fourth member of the Shahejie Formation in the Bonan Depression, Bohai Bay Basin, and found that it is characterized by a lack of bottom water, inverted oil-gas interface, tight reservoir, high formation pressure and close contact between source rocks and reservoirs, thus confirming that it is a continuous petroleum reservoir. Taking the geological conditions of the Triassic Chang-7 tight oil reservoir in the Ordos Basin as constraints, Zhang et al. (2016) utilized hydrocarbon generation and accumulation simulation to analyze the accumulation mechanism and found that the hydrocarbon generation expansion force is the key force for tight oil accumulation. According to the method of accumulation, Zhao et al. (2016) classified petroleum reservoirs into continuous (shale oil and gas and coalbed gas), quasi-continuous (tight oil and gas) and discontinuous (conventional oil and gas) hydrocarbon accumulations. Pang et al. (2020, 2021a, 2021b) investigated the correlation between conventional and unconventional petroleum resources, clarified the difference between their accumulation dynamics and proposed a unified accumulation model; however, these were obtained by basin tectonic evolution and source rock-reservoir assemblage characterization and lacked the support of real data.

Li et al. (2017) analyzed the geological and geochemical characteristics of tight petroleum reservoirs in the lower third member of the Shahejie Formation in the Shulu Sag, Bohai Bay Bain and found that it has the characteristics of a wide distribution and a tight reservoir, confirming that it is a continuous petroleum reservoir. Larue et al. (2018) evaluated the unconventional hydrocarbon resources in the deep San Joaquin Valley Basin, California, and classified them into two categories: UR-I and UR-II. Type UR-I, which accumulates under buoyancy, refers to tight petroleum reservoirs distributed in structural and stratigraphic traps with unified oil-gas-water interfaces and pressure systems, and this type is similar to "accumulation before reservoir densification" (Jiang et al., 2006) and "conventional tight petroleum reservoirs" (Pang et al., 2014b). Type UR-II, which mainly accumulates under no buoyancy, refers to tight petroleum reservoirs with a wide range of distributions in slope and sag locations, and this type is similar to continuous petroleum reservoirs (Schmoker, 1995), "accumulation after reservoir densification" (Jiang et al., 2006) and "deep basin tight oil and gas reservoirs" (Pang et al., 2014b).

2.4. History of DCHA studies in the Dongpu Depression, Bohai Bay Basin, China

The study of tight petroleum reservoirs in the Dongpu Depression began in 1991 (Xu, 1991), and many types of petroleum reservoirs have been discovered. Specifically, as the structural location deepens (from high to slope to sag), the petroleum phases and oil-gas-water interfaces change in order (see Section 1), and the reservoir tightness and trap types change from conventional faults and lithological traps to tight lithological traps and to continuous tight petroleum reservoirs without traps. This is a typical DCHA, which is superimposed in the vertical direction and compounded in the horizontal direction and has enormous potential for further petroleum exploration. The geological features of the DCHA are remarkably similar to those of the "sag-wide oil-bearing theory" (Zhao et al., 2004), "two types of tight sandstone gas reservoirs" (Jiang et al., 2006) and "superimposed continuous petroleum reservoirs" (Pang et al., 2014b; Pang et al., 2014b). However, there are also obvious differences in geological characteristics compared with those of deep basin gas (Masters, 1979), basin centered gas accumulation (Rose, 1981), "continuous petroleum accumulation" (Schmoker, 1995), "source-contacting gas" (Zhang, 2003), "quasi-continuous petroleum reservoirs" (Zhao et al., 2013) and "continuous petroleum reservoirs". In addition, DCHAs are common in petroleum-rich depressions in the Bohai Bay Basin, China (Cheng et al., 2015; Liu, 2015a, 2015b; Zhao, 2012; Zhao et al., 2004) and San Joaquin Valley, USA (Larue et al., 2018). Previous studies on the formation mechanism and distribution patterns of DCHAs have achieved significant progress. However, the intrinsic and substantial relationships among the different types of petroleum reservoirs in DCHAs in different structural locations remain unclear.

3. Geological setting of the Dongpu Depression, Bohai Bay Basin, China

The Bohai Bay Basin is one of the most abundant petroleum-bearing basins in China and East Asia. The Dongpu Depression is located in the Linqing Subbasin in the southeastern Bohai Bay Basin (Fig. 2c) (Hu et al., 2021a; Matthews et al., 2016; Wang et al., 2015). It is a Cenozoic continental rifted lake basin with Paleozoic-Mesozoic strata (Su et al., 2006), an NNE trend and an area of approximately 5.3×10^3 km^2. The Dongpu Depression is wide in the north and narrow in the south, is

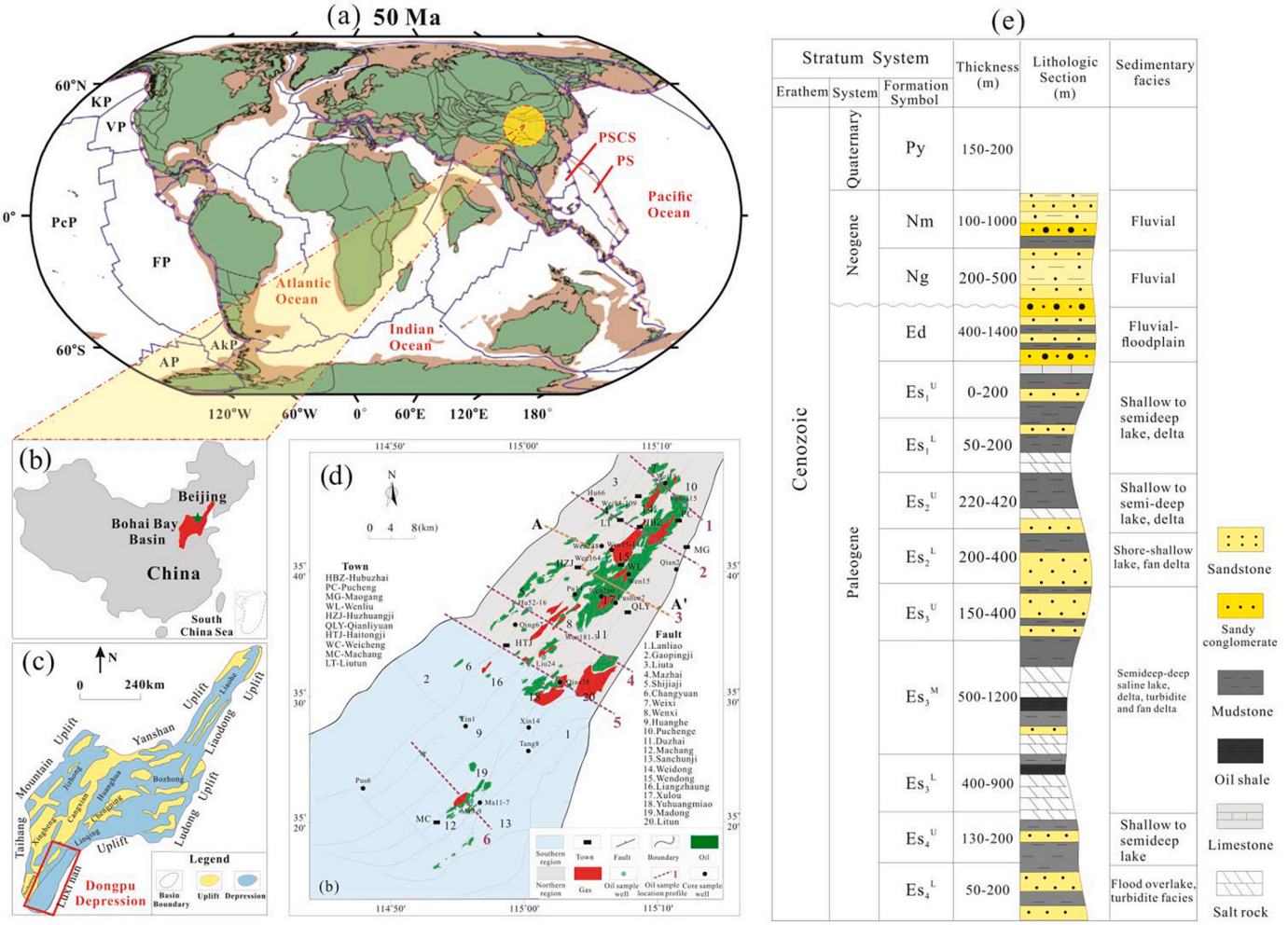

Fig. 2. (a) Tectonic location of the Bohai Bay Basin in 50 Ma on Earth (Matthews et al., 2016); (b) Overview map of China showing the location of Bohai Bay Basin; (c) Overview map of Bohai Bay Basin showing the location of Dongpu Depression (Hu et al., 2021a, 2021b); (d) Distribution of faults (middle of the third member of Shahejie Formation) and fields in the Dongpu Depression, modified after Hu et al. (2022); (e) Generalized Paleogene stratigraphy of the Dongpu Depression. Py: Pingyuan Formation; Nm: Minghuazhen Formation; Ng: Guantao Formation; E_3d: Dongying Formation; E_2s: Shahejie Formation; $E_2s_1^U$: Upper sub-member of first member of E_2s; $E_2s_1^L$: Lower sub-member of first member of E_2s; $E_2s_2^U$: Upper submember of second member of E_2s; $E_2s_2^L$: Lower sub-member of second member of E_2s; $E_2s_3^U$: Upper sub-member of third member of E_2s; $E_2s_3^M$: Middle sub-member of third member of E_2s_3; $E_2s_3^L$: Lower sub-member of third member of E_2s_3; $E_2s_4^U$: Upper sub-member of fourth member of E_2s; $E_2s_4^L$: Lower sub-member of fourth member of E_2s_4.

bounded by the Luxi Uplift in the east, and overlies the Neihuang Uplift in the west, the Lankao Uplift in the south, and the Xinxian Sag in the north. The Dongpu Depression is mainly composed of the western slope belt, western sag belt, central uplift belt, eastern sag belt and eastern steep slope belt (Fig. 2d) (Hu et al., 2021b; Liu and Jiang, 2013; Su et al., 2006). The DCHA discovered in the eastern Wenliu area is the most petroleum-enriched area in the Dongpu Depression, with an area of approximately 650 km^2. The eastern Wenliu area is composed of a rolling anticline belt, a graben belt, a reverse roof belt and the Qianliyuan Sag. Consistent with the overall structural evolution of the Dongpu Depression, the eastern Wenliu area experienced two key stages: the Paleogene rift stage and the Neogene-Quaternary depression stage (Su et al., 2006). The Shahejie Formation (Es) developed in the former stage, which is subdivided into the initial rifting period, strong rifting period, shrinking period and declining period, corresponding to sedimentation of the lower fourth member of the Es (Es_4^L), upper fourth member (Es_4^U) - third member of the Es (Es_3), second member (Es_2) - first member of the Es (Es_1), and Dongying Formation (Ed), respectively. Es consists of the Es_4, Es_3, Es_2 and Es_1 members (Fig. 2e), in which the Es_4 has an angular unconformable contact with Mesozoic strata and Es_1 conformably contacts the overlying Ed.

Specifically, Es_4^L consists of fluvial facies, which are composed of thin interbeds of purplish red, gray shale and light brown sandstone. Es_4^U is composed of thin interbeds of gray and dark gray shale and sandstone, in which thick gypsum salt rocks are developed in some northern areas. Es_3 includes Es_3^U, Es_3^M and Es_3^L. Es_3^L consist of gray and dark gray shale, which are interbedded with siltstone with different thicknesses, and thick gypsum salt rock is developed on the top. Es_3^M is composed of gray and dark gray mud shale, brown oil shale, gray siltstone, gypsum-bearing mudstone, and mudstone intercalated with gray thinly layered calcareous siltstone. Thick gypsum salt rock is developed on the top of the eastern Wenliu area. Es_3^U is composed of gray and dark gray shale, which are interbedded with siltstone of different thicknesses. Es_2 is a set of normal cycle deposits overall, in which Es_2^L is composed of thin interbeds of red sandstones and mudstone with strong heterogeneity, while the Es_2^U is composed of red gypsum-bearing mudstone. The Es_1 is composed of gray and dark gray shale, which are interbedded with siltstone of different thicknesses, and a set of regional thick gypsum salt rocks is developed at the bottom.

Currently, 1607 exploration wells have been drilled in the Dongpu Depression, and the well control degree is 0.3 wells per square kilometer. The cumulative proven oil and gas geological reserves are 601.0

$\times 10^6$ t and 138.9 $\times 10^9$ m^3, and the proven rates are 48.6% and 37.8%, respectively. In the eastern Wenliu area, the proven oil, dissolved gas, gas, and condensate oil geological reserves are 52.0 $\times 10^6$ t, 13.1 $\times 10^9$ m^3, 2.5 $\times 10^9$ m^3 and 147.0 $\times 10^3$ t, respectively. DCHAs are mainly developed in Es_4, Es_3, and Es_2 and are mostly enriched in Es_3.

Currently, petroleum is found in different structural locations (high, slope, and sag) and different formations (Es_4^U, Es_3^L, Es_3^M, Es_3^U, Es_2, Es_1, and Ed) in the eastern Wenliu area and mainly distributed in the sandstone reservoirs in Es_3^M, Es_3^U, and Es_2^L (Fig. 3). The Es_2^L oil is mainly distributed in the high structural location, the Es_3^U oil is distributed near the Qianliyuan Sag, and the Es_3^M oil is distributed in the structural slope location (Fig. 4). Overall, petroleum in the eastern Wenliu area is superimposed vertically and compounded horizontally with multiple formations and is a typical DCHA.

4. Samples and methods

4.1. Sampling collection

Because DCHAs are widely developed in different structural locations (high, slope, and sag) and different formations in the eastern Wenliu area, and the effective source rocks in the Dongpu Depression mainly include the Es_4^U and Es_3^L laminated shale (Hu et al., 2022), sampling strictly followed three principles: 1) sampled wells were located in a section that cuts across the key structure; 2) for the selected cross-section, oil and sandstone cores in different structural locations were selected; and 3) for the selected cross-section, oil and sandstone cores in different formations were selected (Figs. 3 and 4). Based on these principles, 13 and 20 cores were obtained in oil and sandstone, respectively.

4.2. Experimental methods

Soxhlet extraction was performed on the shale samples for 72-h to obtain the extracts. Saturated hydrocarbons and aromatic hydrocarbons in crude oil were separated by silica gel chromatography. Saturated hydrocarbons in the shale extracts were separated for gas chromatography (GC) and gas chromatography–mass spectrometry (GC–MS) analysis. An HP 6890 chromatograph (30 m × 0.32 mm) with nitrogen as the carrier gas was used for the GC analysis. An Agilent 5973I instrument with helium as the carrier gas and an HP 6890 chromatograph (30 m × 0.32 mm) were used for the GC–MS analysis.

Total scanning fluorescence (TSF) is a quantitative fluorescence technique (QFT) (Liu et al., 2016). A Varian Cary-Eclipse fluorescence spectrophotometer fitted with a customized sampling phase was used for TSF analysis (Liu and Eadington, 2005). The diluted crude oil samples were illuminated with an excitation wavelength step of 2 nm. The scanning range was from 220 to 340 nm. At the same time, the synchronous scan function of the spectrophotometer was used to record the emission spectra with a wavelength range of 250–540 nm, and then the three-dimensional fluorescence spectrum was obtained (Liu et al., 2014b).

An Olympus AX70 microscope with transmitted light and a UV light source was used to analyze the hydrocarbon-bearing inclusion petrography of sandstone samples. The UV excitation fluorescence characteristics of the inclusions were obtained by a mercury lamp and a 400 nm filter, and the emission fluorescence wavelength was >400 nm (Liu et al., 2013).

The homogenization temperature data of saline fluid inclusions associated with hydrocarbon-bearing inclusions were analyzed using a Linkam TH-600 heating-freezing phase mounted on the microscope (Liu et al., 2013; Wilkinson et al., 1998). Before the experiment, the heating-freezing phase system was tested and calibrated with standard samples. The homogenization temperature data were measured by the cyclic test method (Goldstein, 1994). The heating rates were 10 °C/min and 1 °C/min, and the accuracies were 1 °C and 0.1 °C, respectively.

A JS-3 rock porosity casting instrument was used to fabricate thin casting sections. The preparation process can be found in Bao and Wu (2019). The thin sections were then placed under a polarizing microscope for direct observation. The sandstone samples were treated following the method from Loucks et al. (2009) for SEM imaging using an FEI Quanta 200 F scanning electron microscope at 20 kV and a work distance of 10 mm. Porosity and permeability data were collected from the Zhongyuan Oilfield, and the testing process was based on Min et al. (1999).

5. Results

5.1. Petrology of sandstone

5.1.1. Lithology

The Es in the Dongpu Depression mainly includes sandstone, sandy conglomerate, mudstone, oil shale and dolomite, among which there are four sets of gypsum-salt rocks (Fig. 2e). The sand body thickness of the Es in the eastern Wenliu area is thin, in the range of 1–4 m. Analyses of 2858 sandstone core samples showed that the reservoirs of the eastern Wenliu area in different structural locations and strata are mainly siltstone, followed by fine sandstone. In detail, the ratios of siltstone account for 97.5%, 95.2%, 99.6% and 100% in the Es_2, Es_3^U, Es_3^M and Es_3^L sandstones, respectively.

5.1.2. Porosity and permeability

The porosity and permeability of 2858 Es sandstones are highly variable (Fig. 5a). The porosity of 86.5% of the Es_2 sandstone is between

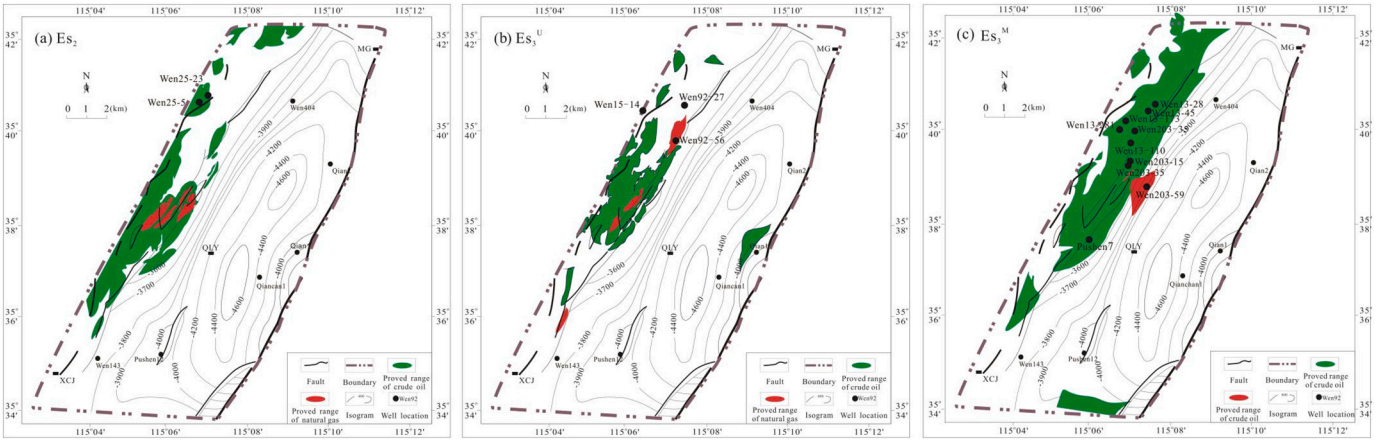

Fig. 3. Petroleum reservoir and selected sandstone core distribution in the eastern Wenliu areaeastern Wenliu area, Dongpu Depression.

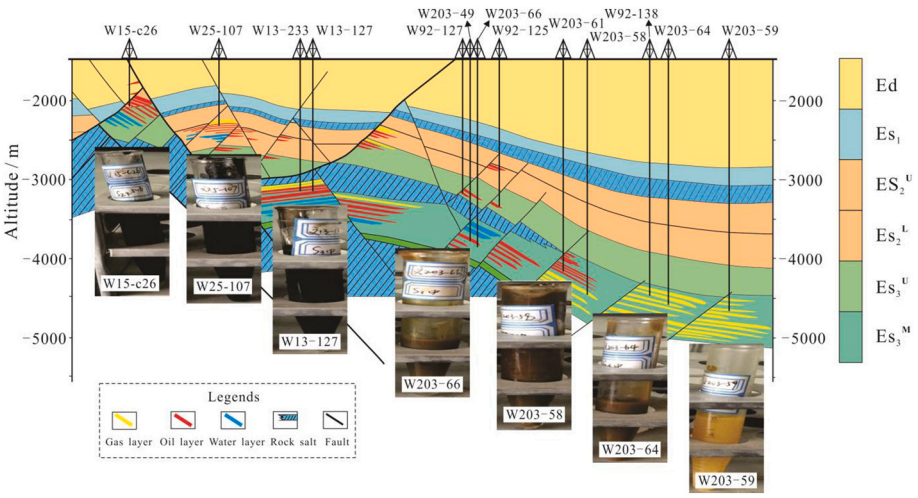

Fig. 4. Stratigraphic cross-section and locations of sampled oil of DCHA in the Es of eastern Wenliu areaeastern Wenliu area, Dongpu Depression.

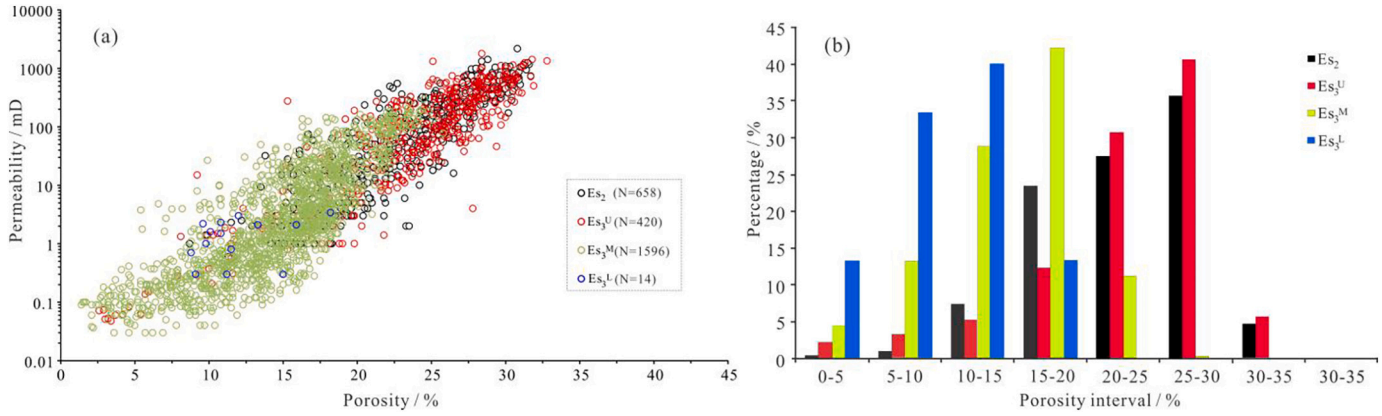

Fig. 5. Correlation between porosity and permeability (a) and frequency histograms of porosity (b) in different Es sandstones of eastern Wenliu areaeastern Wenliu area, Dongpu Depression.

15% and 30%. The porosity of 83.6% of the Es_3^U sandstone is between 15% and 30%. The porosity of 71.0% of the Es_3^M sandstone is between 10% and 20%. The porosity of 73.3% of the Es_3^L sandstone is between 5% and 15% (Fig. 5b). Analyses showed that as the depth increases, the percentage of the sandstone with low porosity increases gradually. Generally, the porosity and permeability of tight sandstone are <10% and 0.1 mD, respectively (Guo et al., 2017). The Es_2 sandstones consist of 1.3% tight sandstone, and the percentages of tight sandstone in the Es_3^U, Es_3^M and Es_3^L sandstones are 5.5%, 17.6% and 46.7%, respectively.

5.1.3. Pore types

The pore types of the Es sandstone in the eastern Wenliu area are diverse. As shown in Fig. 5a, there is a high correlation between the porosity and permeability of the sandstone samples, indicating that the reservoir space is mainly pores. Light microscopy and scanning electron microscopy observations of the thin sections show that the pores are primary, secondary, and mixed pores, with less developed fractures.

The primary intergranular pores are mainly developed in the Es_2 sandstone (Fig. 6a, b). Due to the large depth, the Es_3 sandstone underwent a strong transformation process of compaction, cementation, dissolution, metasomatism and redissolution, with only a few primary pores remaining. Secondary pores are the main pore types in the Es_3 sandstone, including intergranular and intragranular dissolved pores. The former refers to pores formed by the dissolution of cements and matrix bases at or between grain edges, such as dissolved pores at feldspar grain edges (Fig. 6c) and large dissolved intergranular pores (Fig. 6d), which are the most important pore types in the Es_3 sandstone. Intragranular dissolved pores of feldspar are the main pores (Fig. 6e). Mold pores are formed under strong dissolution, with the same shape as the original components (Fig. 6f). Mixed pores, which refer to pores composed of primary pores and secondary pores and are the combination of secondary pores and primary pores formed by the corrosion of particle edges or the corrosion of particle cements (Figs. 6g-h). Fractures are less developed in the study area. Structural fractures are developed in the high structural location, and diagenetic fractures are mostly developed in the slope and sag (Fig. 6i).

5.1.4. Diagenesis

The diagenetic processes in the eastern Wenliu area include compaction, cementation, and dissolution, which are the key factors affecting the evolution of porosity and permeability in the sandstone. Compaction has resulted in three features: 1) local bending deformation of plastic mineral particles such as mica (Fig. 7a); 2) cracked or broken brittle mineral particles such as quartz (Fig. 7b); and 3) visible seam contacts when the compaction is tight (Fig. 7c). Cementation has produced cement, which occupies primary pores, resulting in throat thinning and pores decreasing. The cementation in the eastern Wenliu area is mostly late carbonate cementation (Fig. 7d). Cementation also includes clay minerals and iron cementation; the former is distributed closely to clastic particles in a ring pattern (Fig. 7e), and the latter is mostly distributed in the form of raspberry ball aggregates adjacent to detritus particles (Fig. 7f). Dissolved pores formed by dissolution

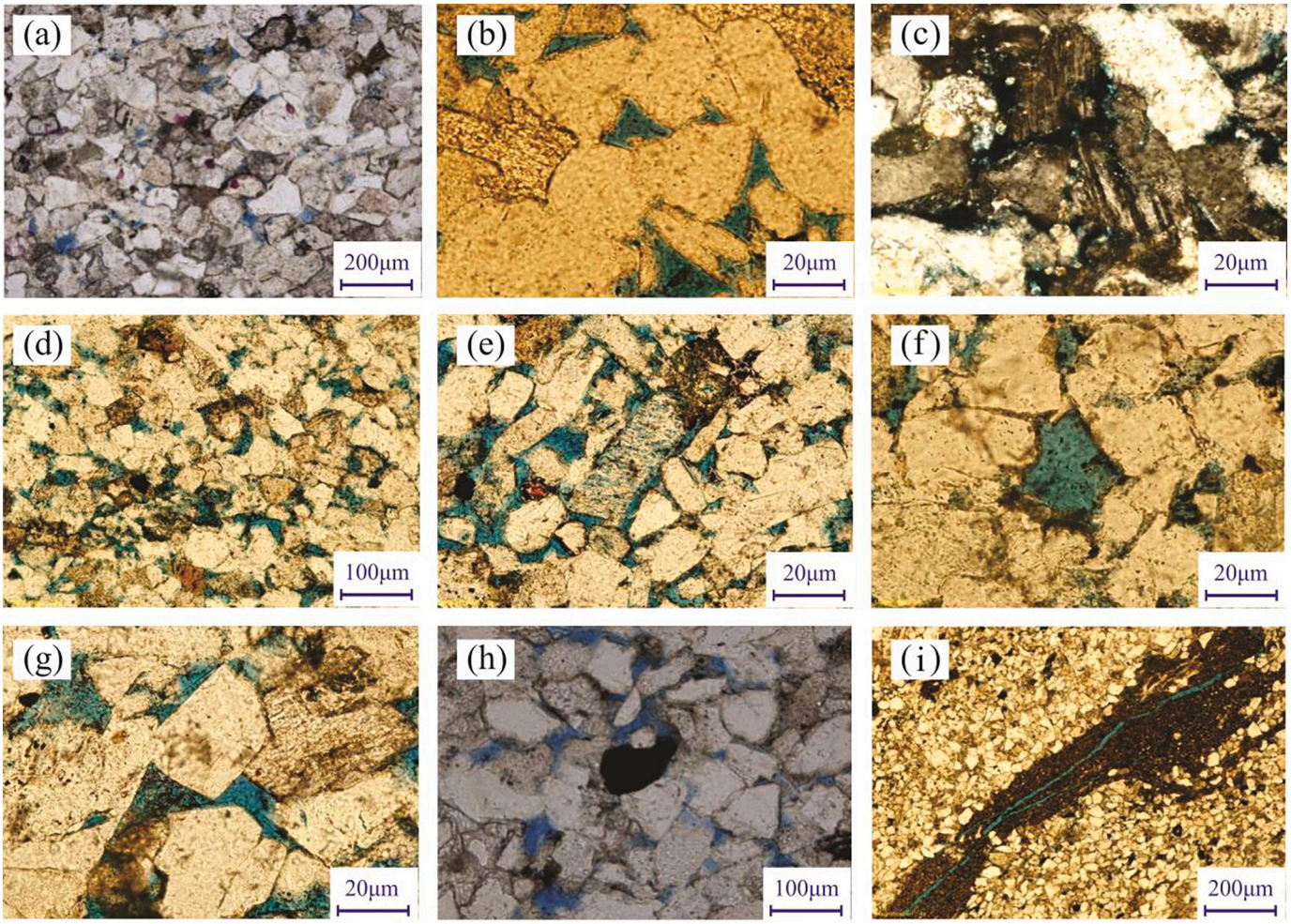

Fig. 6. Pore types of sandstone in Es sandstones of eastern Wenliu areaeastern Wenliu area, Dongpu Depression. (a) Wen 13-110, 3546.28m; (b) Wen 146, 2885.98m, residual intergranular pore; (c) Wen 203-59, 4182.91m, dissolution pores at feldspar grain edge; (d) Pushen 7, 3696.7m, inter-granular dissolution pores; (e) Pushen 7, 3665.1m, honeycomb intragranular dissolution pores in feldspar; (f) Wen 203-59, 4182.91m, mold pore; (g) Wen 203-15, 3572.05m, mixed pores; (h) Wen 220, 3347.8m; (i) Pushen 7, 4156.9m, shrinkage fracture.

commonly connect with primary intergranular pores and mixed pores, which can improve reservoir physical properties. Marginal and intragranular dissolution of feldspars and lithic debris is present (Figs. 7e-f).

5.2. *Petroleum types*

The color of petroleum changes regularly with the burial depth and structural location in the Dongpu Depression. From high to slope to sag locations, the oil color varies from black (wells Wen 15-c26 and Wen 25–107) to brown (well Wen 13–12), to yellowish brown (wells Wen 203–66, Wen 203–58 and Wen 203–64), and to light yellow (well Wen 203–59) (Fig. 4). According to the phase states, reservoir densification, reservoir formation pressure, and oil-gas-water interfaces, the petroleum reservoirs can be divided into the following types (Jiang and Cha, 2005; Lu, 2008).

1) **Conventional black heavy oil sandstone reservoir at the upper high structural location**. The Wen 15 and Wen 25 petroleum reservoirs are located in Es_2 in a high structural location, with shallow burial depths ranging from 2338 to 2461 m. The interpreted logging porosity of the sandstone reservoirs ranges from 15.2%–26.3%, with an average of 21.2%, and these reservoirs are conventional reservoirs. The formation pressure coefficient ranges from 0.97 to 1.22, with an average of 1.15, and it has normal-weak overpressure. The oil-gas-water interface is normal (gas at the top, oil at the center and water at the bottom) (Fig. 4). The oil density of Wen 15 is 0.863 g/cm^3, with a GOR of 59. The oil density of Wen 25 is 0.847 g/cm^3, with a GOR of 56.
2) **Conventional brown light oil sandstone reservoir at the lower structural high location.** The Wen 13 petroleum reservoir is located in Es_3^M in the lower structural high location, with depths ranging from 3132 to 3483 m. The logging porosity of the sandstone reservoir is between 11.9% and 21.5%, with an average of 15.2%, and this reservoir is a conventional reservoir. The formation pressure coefficient is 1.12, with normal pressure. The oil-gas-water interface is normal (Fig. 4). The oil density of Wen 13 is 0.828 g/cm^3, with a GOR of 242.
3) **Unconventional (tight) yellow-brown overpressure light/volatile oil sandstone reservoir at the structural slope location**. The Wen 203 and Wen 200 petroleum reservoirs are located in Es_3^M in structural slope locations, with depths ranging from 3569 to 3824 m. The logging porosity of sandstone reservoirs is between 5.9% and 13.2%, with an average of 9.1%, and these reservoirs are tight reservoirs. The formation pressure coefficient is between 1.32 and 1.59, with an average of 1.46, and it has overpressure. The oil-water interfaces of the Wen 203 and Wen 200 petroleum reservoirs are inverted (water at the top and oil at the bottom) (Fig. 4). The oil density of Wen 203 is 0.825 g/cm^3, with a GOR of 284. The oil

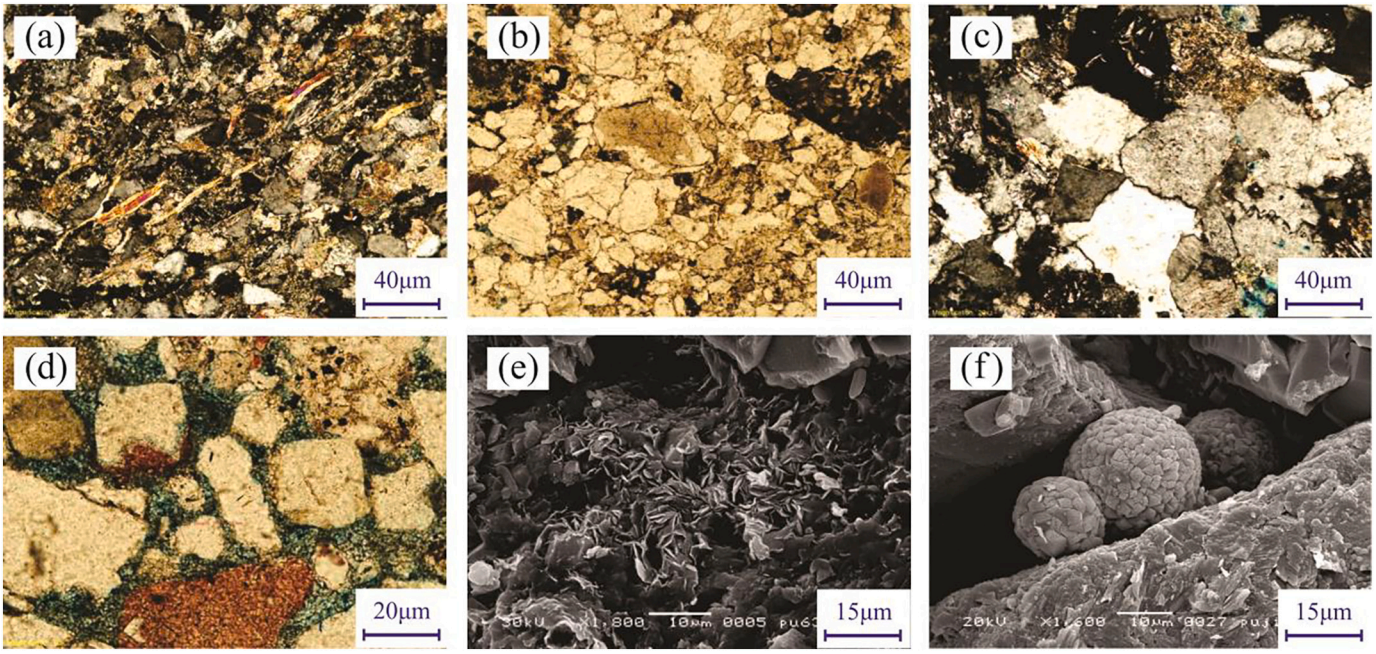

Fig. 7. Microscopy images showing the pore characteristics of Es sandstone of eastern Wenliu area, Dongpu Depression. (a) Pushen 7, 4156.9m, mica directional arrangement and local bending; (b) Wen 203-59, 4182.91m, quartz cracks; (c) Wen 203-59, 4182.91m, stylolite contacts of quartz; (d) Wen 203-35, 3362.82m, ankerite cementation; (e) Wen 203-15, 3334.40m, flake chlorite; (f) Wen 146, 2360.96m, strawberry-shaped pyrite aggregate.

density of Wen 200 is 0.795 g/cm^3, with a GOR of 387. Wen 203 is a brown tight overpressure light oil reservoir. Wen 200 is a yellow-brown tight overpressure volatile oil reservoir.

4) **An unconventional (tight) overpressure condensate gas reservoir containing light yellow condensate oil at the structural sag location.** The Wen 203–58 and Wen 203–59 petroleum reservoirs are located in Es_3^M in the structural sag location, with depths ranging from 4109 to 4265 m. The logging porosity of the sandstone reservoirs is between 2.1% and 14.0%, with an average of 7.6%, and these reservoirs are tight reservoirs. The formation pressure coefficient is 1.78, representing a strong overpressure. The oil-gas interface of the Wen 203–58 petroleum reservoir is inverted (oil at the top and gas at the bottom), and there is no gas-water interface in the Wen 203–59 petroleum reservoir (Fig. 4). The oil density of Wen 203–58 is 0.788 g/cm^3, with a GOR of 3141. The oil density of Wen 203–59 is 0.784 g/cm^3, with a GOR of 13,158.

The DCHA in the Dongpu Depression is composed of Es_2, Es_3^U, and Es_3^M petroleum. Petroleum distribution patterns in different strata are different, and there are clear differences in petroleum reservoirs in different structural locations, even within the same stratum. Specifically, Es_2 petroleum is mainly distributed in the high structural location, Es_3^M petroleum is mainly distributed in the slope and sag locations, and Es_3^U petroleum is mainly distributed in the slope location. Conventional black heavy oil sandstone reservoirs are mainly developed at the upper high structural location, conventional brown light oil sandstone reservoirs are mainly developed at the lower structural high location, tight yellow-brown overpressure light/volatile oil sandstone reservoirs are mainly developed at the structural slope location, and tight overpressure condensate gas reservoirs containing light yellow condensate oil are mainly developed at the structural sag location. With the increase of the depth of strata (high to slope to sag), the petroleum distribution locations gradually migrate to the sag center, and the DCHA shows an obvious petroleum sequence: from conventional black heavy oil reservoirs to conventional brown light oil reservoirs, to tight brown overpressure light oil reservoirs, to tight yellow-brown overpressure volatile oil reservoirs, and finally to tight overpressure condensate gas reservoirs (Fig. 4).

5.3. Hydrocarbon fluid inclusions

5.3.1. Petrographic features

Transmitted light and fluorescence observation results of 20 sandstone reservoir samples show that the fluorescence colors of hydrocarbon fluid inclusions are mainly yellow and blue, including yellow, yellow-white, yellow-green, blue-green and blue-white (Figs. 8–12).

The fluorescence colors of hydrocarbon inclusions in sandstone at different structural locations and strata are different. For the high structural location, the colors of the hydrocarbon inclusions in the Es_2 and Es_3^U sandstones at higher locations are yellow, yellow-white, and yellow-green, accounting for 41.2%, 47.1%, and 11.8%, respectively (Fig. 8), whereas for deep the Es_3^M sandstone, the colors of the hydrocarbon inclusions include yellow and blue, and the proportions of the two are similar. Yellow, yellow-white, yellow-green, blue-green, and blue-white colors accounted for 3.6%, 7.1%, 32.1%, 17.9% and 39.3%, respectively (Fig. 9). For the structural slope location, the hydrocarbon inclusion colors in the Es_3^U sandstone include yellow and blue, with yellow dominating and the proportions of yellow, yellow-white, yellow-green and blue-white are 5.0%, 35.0%, 45.0% and 15.0%, respectively (Fig. 10). All the hydrocarbon inclusion colors in the Es_3^M sandstone on the slope are blue-white (Fig. 11). For the sag location, all the inclusion fluorescence colors in the Es_3^M and Es_3^L sandstones are blue-white (Fig. 12).

The distribution characteristics of the hydrocarbon inclusions in sandstone in the different structural locations and strata are also different. For the high structural location, most inclusions occur sporadically in the internal dissolution pores of quartz and feldspar, or in quartz secondary enlargement, accounting for 51.2%, 13.1%, and 14.3%, respectively (Figs. 8–9). For the slope location, the Es_3^U inclusions are mainly distributed in groups and are bead-like in the internal dissolution pores of quartz and intragranular fractures of quartz, and the former accounts for 85.7% (Fig. 10). The Es_3^M inclusions are all developed in quartz intragranular fractures and quartz cracks, distributed in clusters and are bead-like (Fig. 11). For the sag location, hydrocarbon

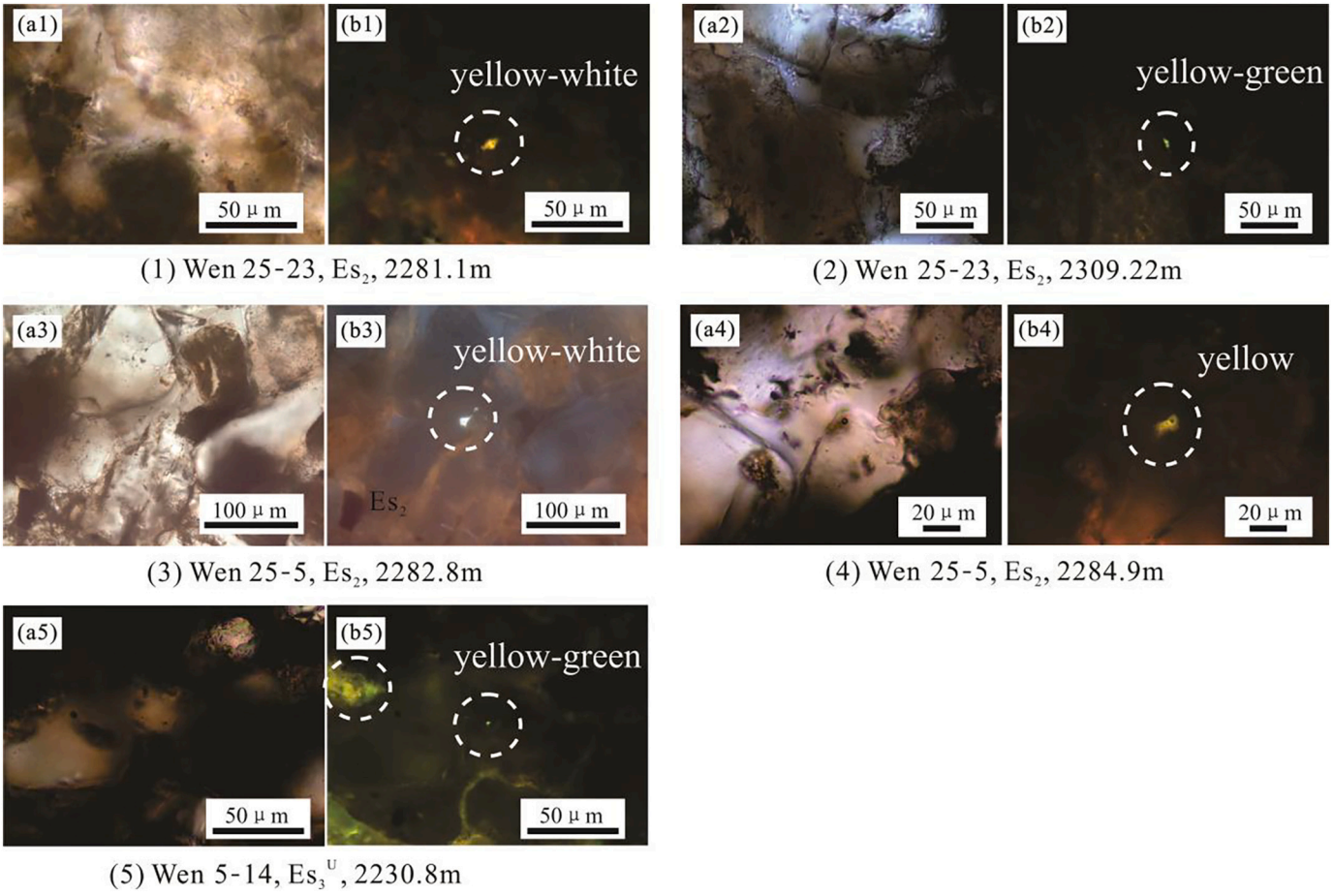

Fig. 8. Petroleum fluid inclusion images of Es_2 and Es_3^U sandstones in structural high position in DCHA of eastern Wenliu area, Dongpu Depression.

inclusions in Es_3^M and Es_3^L are all developed in the quartz intragranular fractures and cracks of quartz, distributed in clusters and bead-like (Fig. 12).

5.3.2. *Homogenization temperatures*

The homogenization temperatures of brine inclusions (HTBIs) associated with the hydrocarbon inclusions in the sandstone at different structural locations and in different strata are different. For the upper shallow structural location, the HTBIs associated with yellow fluorescent hydrocarbon inclusions in the Es_2 (Wen 25–23) and Es_3^U (Wen 15–14) sandstones are 72 °C–86 °C and 94 °C–117 °C, respectively. For the deep high structural location, the HTBIs associated with yellow and blue fluorescent hydrocarbon inclusions in the Es_3^M sandstone (Wen 13–281) are 127 °C–136 °C and 115 °C–132 °C, respectively, and the HTBIs associated with the yellow and blue fluorescent hydrocarbon inclusions in the Es_3^M sandstone (Wen 13–110) are 140 °C–153 °C and 123 °C–141 °C, respectively. For the slope location, the HTBIs associated with the yellow and blue fluorescent hydrocarbon inclusions in the Es_3^U sandstone (Wen 92–56) are 107 °C–123 °C and 87 °C–103 °C, respectively. The HTBIs associated with the yellow and blue fluorescent hydrocarbon inclusions in the Es_3^M sandstone (Wen 203–35) are 111 °C–133 °C. For the sag location, the HTBIs associated with the blue fluorescent hydrocarbon inclusions in the Es_3^M sandstone (Wen 203–59) are within 119 °C–153 °C. The HTBIs associated with the blue fluorescent hydrocarbon inclusions in the Es_3^L sandstone (Pushen 7) are 127 °C–148 °C.

5.4. *Oil biomarkers*

GC analyses of saturated hydrocarbons in oil show that the distribution of n-alkanes remains intact in different structural locations and different strata (Fig. 13), and no C_{25}-norhopane compounds were detected (Figs. 14a, 15a and 16a), indicating no obvious biodegradation (Peters and Moldowan, 1993). The light hydrocarbon components of n-alkanes increase gradually as the depth increases (Fig. 13) and are characterized by low pristane, high phytane, and high gammacerane contents (Figs. 13–16).

GC–MS analyses of saturated hydrocarbons in oil showed that the terpene distribution characteristics in the different strata are similar, but the abundance and distribution characteristics of the terpene in the oil at different depths are significantly different. As the depth increases, the terpene abundance decreases, and the "bulge" phenomenon is more significant, such as in the deeper Wen 203–59, Wen 203–64, and Wen 203–58 wells (Figs. 14a, 15a and 16a). The sterane distribution characteristics in the different strata are similar, but the abundance and distribution characteristics of the sterane at different depths are obviously different. With increasing depth, the sterane abundance decreases, the relative content of rearranged sterane increases, and the "bulge" phenomenon is more significant (Figs. 14b, 15b and 16b). The sterane indices of C29-ααα-20S/(20S + 20R) and C29-αββ/(αββ + ααα) are within the ranges of 0.17–0.69 and 0.31–0.67, with averages of 0.46 and 0.50, respectively. The higher the oil maturity is, the lower the abundance of terpenes and steranes is, the more obvious the "bulge" phenomenon (Mackenzie, 1984; Peters and Moldowan, 1993), and the higher the content of rearranged steranes is.

GC–MS analyses of aromatic hydrocarbons showed that abundant methyl phenanthrene compounds are present in the oil samples (Figs. 17a, 18a and 19a; Figs. 17b, 18b and 19b), but the calculated methyl phenanthrene index (MPI = 1.5 × (3-MP + 2-MP)/(P + 9-MP + 1-MP)) of the oil from different structural locations and strata distributes

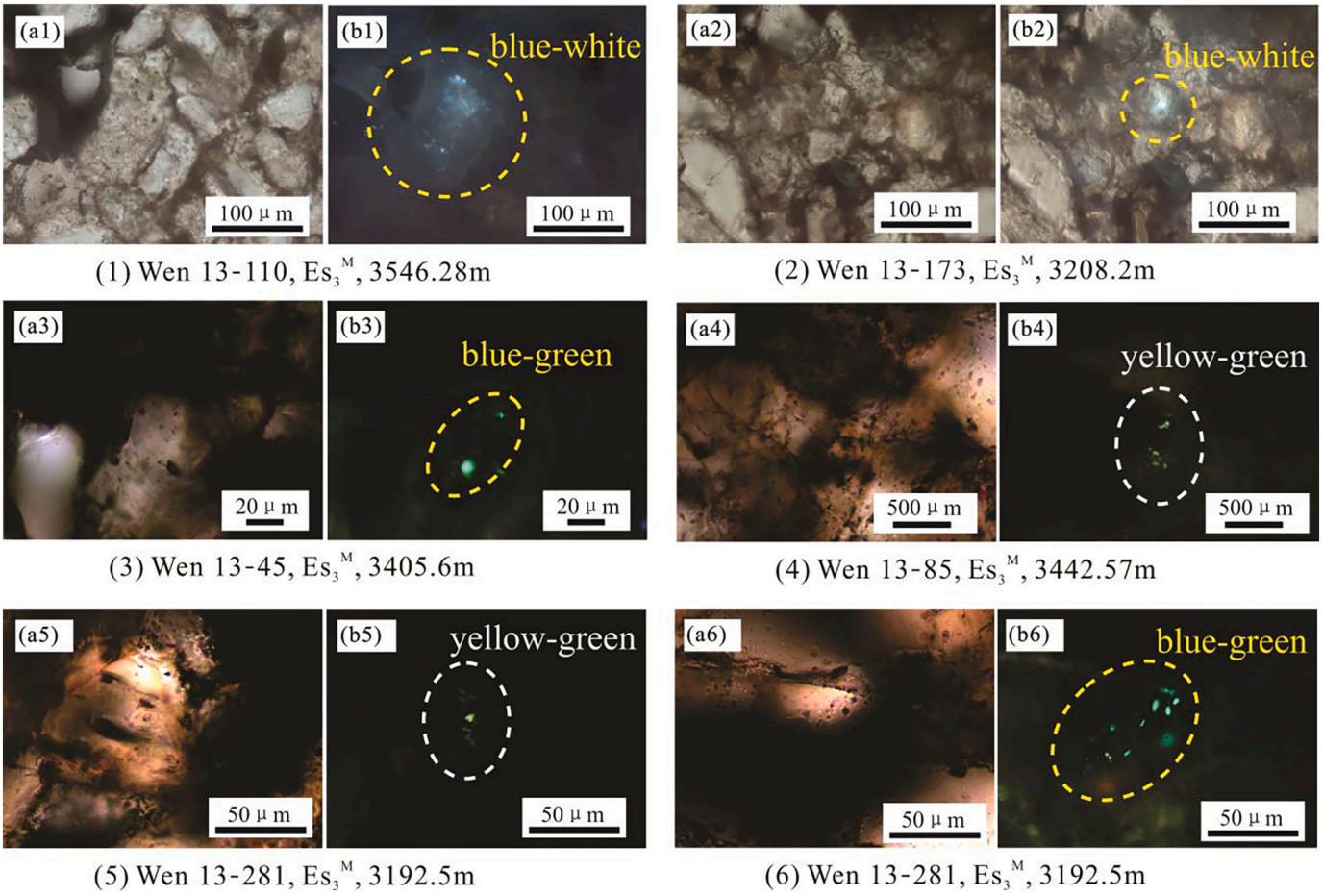

Fig. 9. Petroleum fluid inclusion images of Es_3^M sandstones in the high structural position in DCHA of eastern Wenliu area, Dongpu Depression.

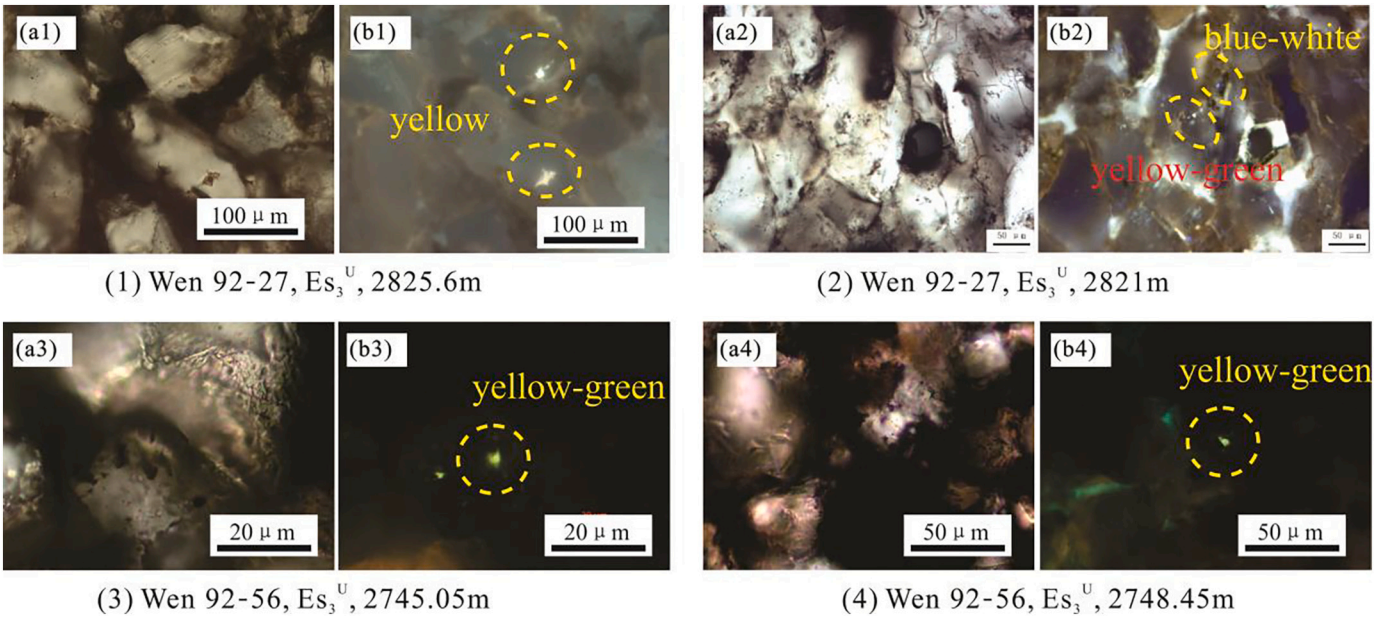

Fig. 10. Petroleum fluid inclusion images of Es_3^U sandstones in structural slope position in DCHA of eastern Wenliu area, Dongpu Depression.

in a narrow range of 0.52–0.70 with only one MPI value >1 (well Wen 203–59) (Fig. 20a). Abundant dibenzothiophene compounds are present in the oil (Figs. 17c, 18c and 19c). The 4,6-dimethyl-dibenzothiophene/1,4-dimethyl-dibenzothiophene (4,6-MDBT/1,4-MDBT) values of the Es_2 and Es_3^M oil in the high structural location are similar and in the ranges of 0.79–0.91 and 0.67–0.88, respectively. The 4,6-MDBT/1,4-MDBT values of the Es_3^U oil in the slope location are within 0.83–0.88 and those of the Es_3^M oil in the slope location are within 1.03–2.23, with

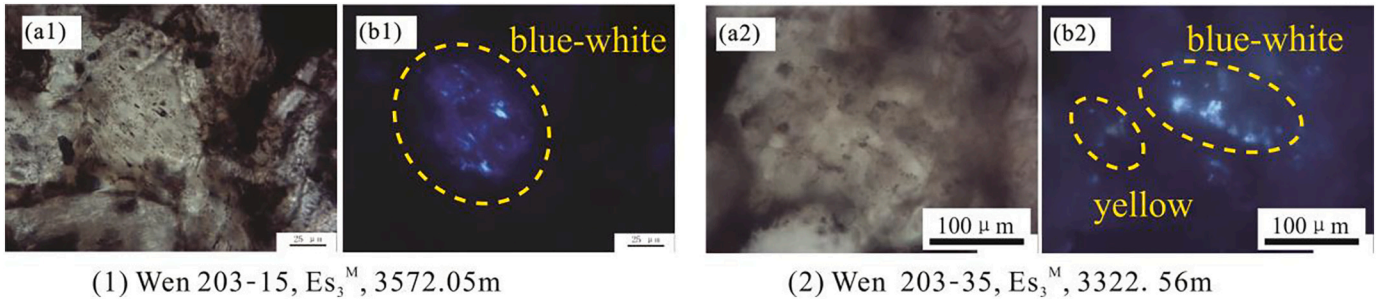

Fig. 11. Petroleum fluid inclusion images of Es_3^M sandstones in structural slope position in DCHA of eastern Wenliu area, Dongpu Depression.

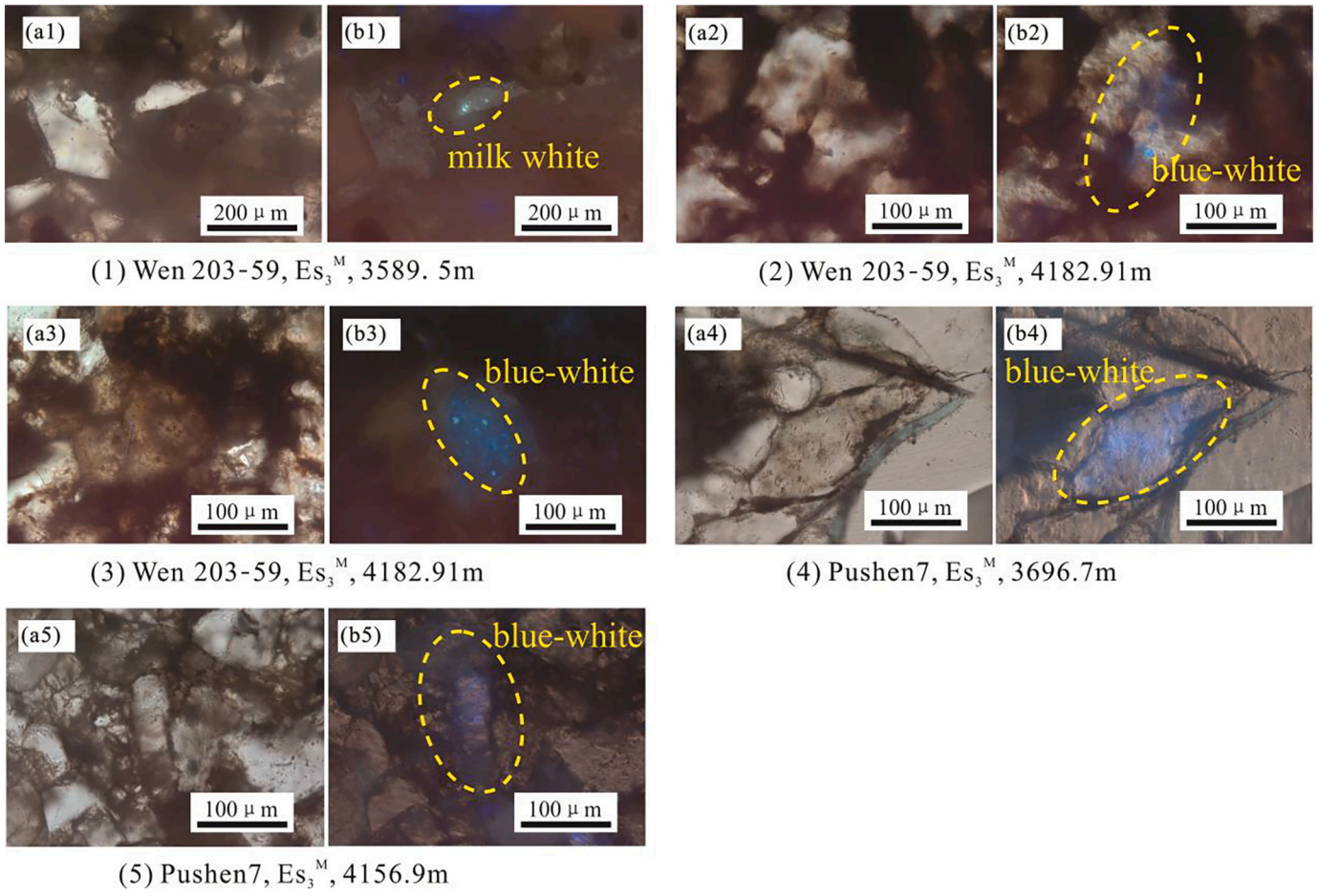

Fig. 12. Petroleum fluid inclusion images of Es_3^M sandstones in structural sag position in DCHA of eastern Wenliu area, Dongpu Depression.

an average of 1.51. The 4,6-MDBT/1,4-MDBT value of the Es_3^M oil in the sag is within 1.04–4.14, with an average of 2.23 (Fig. 20b).

5.5. Quantitative fluorescence analysis

The TSF analysis (Liu et al., 2014a, 2014b, 2014c; Liu et al., 2016; Liu and Eadington, 2005; Liu et al., 2007; Ping et al., 2017) was utilized to analyze the thermal maturity of oil. The results show that the R_1 values (the ratio of the fluorescence intensity at an emission wavelength of 360 nm to the fluorescence wavelength at 320 nm under excitation light of 270 nm) in the TSF fluorescence spectra of the oil at different structural locations and strata are different. Specifically, the R_1 values of the shallow Es_2 and Es_3^U strata and deep Es_3^M strata oil in the high structural location are high, with values of 3.27–3.49, 3.39 and 3.02–3.19, respectively. The R_1 value of the Es_3^U oil in the slope location is 3.26. The R_1 value of the Es_3^M oil in the sag location is the smallest, in the range of 1.74–2.68 (Figs. 20c; 21).

6. Discussion

6.1. Oil thermal maturity

Physical properties such as the color and GOR reflect the maturity of oil. The lighter the color is and the greater the GOR is, the greater the oil maturity is (Jiang and Cha, 2005; Lu, 2008). As shown in Fig. 4, as the depth increases and the structural location deepens (from high to slope to sag), the oil color changes from black to brown to yellow, and finally to light yellow gradually, and the GOR increases gradually, both of which indicate that the oil maturity increases gradually.

Biomarkers such as the sterane indices of C29-ααα-20S/(20S + 20R)

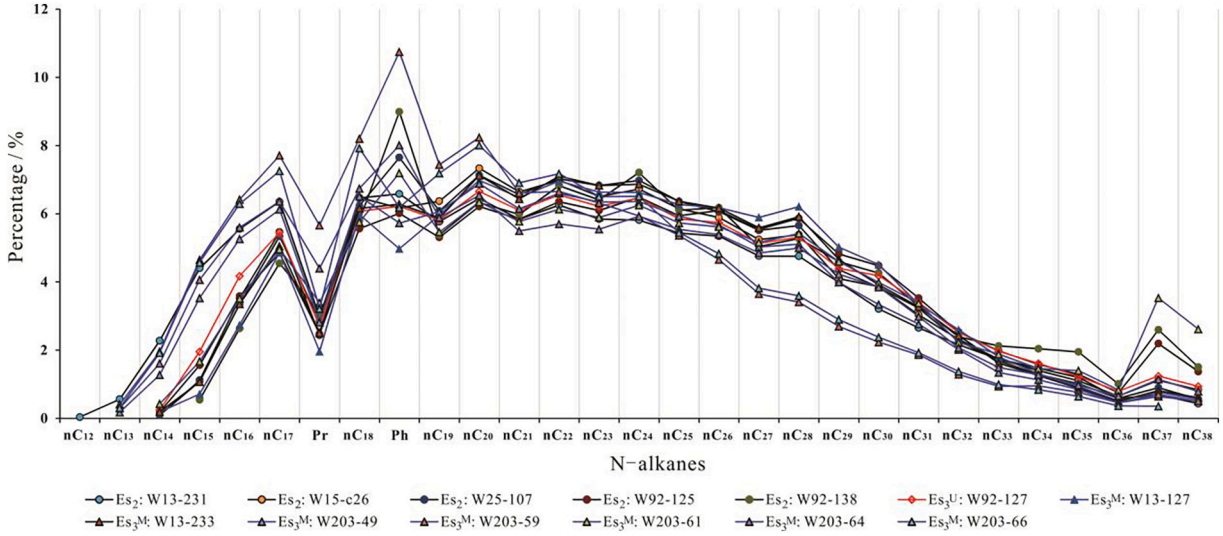

Fig. 13. Distribution characteristics of N-alkanes, Pristine, and Phytane of oil in DCHA of eastern Wenliu areaeastern Wenliu area, Dongpu Depression.

and C29-αββ/(αββ + ααα) can also be used to evaluate the maturity of oil (Peng et al., 2017; Peters and Moldowan, 1993; Tissot and Welte, 1978). As shown in Fig. 22, the maturity of the Es_2 and Es_3 oils in the high structural location increase with increasing depth. The Es_2 and Es_3 oils are low-maturity and mature oils, respectively, and the sterane maturity indices of the Es_3^M oil in the structural slope and sag locations reached equilibrium values (Mackenzie, 1984; Peters and Moldowan, 1993; Seifert and Moldowan, 1986), indicating a high maturity. The n-alkane biomarker contents of highly mature crude oil are very low, and the signal-to-noise ratio of conventional GC–MS analysis is too low to accurately evaluate the type and content of biomarker compounds, resulting in great errors in the biomarker compound index (Peters et al., 2005).

To analyze the maturity of the oil at different structural locations and in different strata, aromatic hydrocarbon indices were utilized in this study, which have wider thermal maturity ranges for thermal maturity evaluation than saturated hydrocarbon indices, were utilized in this study. Radke et al. held that with increasing maturity, the contents of 2-methyl phenanthrene (2-MP) and 3-methyl phenanthrene (3-MP), which have a strong thermal stability in methyl phenanthrene isomers, increase gradually, while the contents of 1-methyl phenanthrene (1-MP) and 9-methyl phenanthrene (9-MP), which have a weak thermal stability, decrease gradually; thus, oil maturity can be assessed by the methyl phenanthrene index (MPI = 1.5 × (3-MP + 2-MP)/(p + 9-MP + 1-MP)) and then the correlation between the MPI and the apparent vitrinite reflectance (R_c) can be established (Radke, 1988; Radke and Welte, 1983; Radke et al., 1990). According to Radke's formula (Radke, 1988), almost all the calculated R_c values are only 0.73%–0.83%, except for that of the oil in Wen 203–59, which is 1.09% (Fig. 20a), contradicting the geological fact that oils with distinct maturities occur in the DCHA, such as light, volatile, and condensate oils at the slope and sag locations. Li and Lin (2005) studied oil maturity in the western sloped area of the Dongpu Depression and found that the methyl phenanthrene index did not change obviously with increasing depth (Li and Lin, 2005). This might be related to oil-generated biota, and the MPI index is commonly suitable for the maturity evaluation of oil generated from type III and type IV kerogen (Lu, 2008; Lu et al., 1996; Zhang and Huang, 1997; Zhu et al., 2009). In addition, the lithology of the source rock has strong effects on the MPI index (Wang and Xia, 1995).

An important aromatic hydrocarbon index in assessing the maturity of oil is 4,6-dimethyl dibenzothiophene/1,4-dimethyl dibenzothiophene (4,6-MDBT/1,4-MDBT) in alkyl dibenzothiophene compounds (Chakhmakhchev et al., 1997; Hughes, 1984). Oil maturity increases with increasing 4,6-MDBT/1,4-MDBT values (Fig. 20b). Analyses show that the oil maturities of the Es_2 and Es_3^M at the high structural location and the Es_3^U at the slope location are similar but are lower than that of the Es_3^M at the slope and sag locations. Moreover, the oil maturity of the Es_2 at the slope and sag locations increase obviously with increasing depth.

The R1 value obtained from quantitative fluorescence analysis is also an indicator of the maturity of crude oil. The greater the R_1 value is, the lower the maturity is (Liu et al., 2014a, 2014b, 2014c; Liu et al., 2016). The R_1 values of the Es_2, Es_3^U and Es_3^M oils from the high structural location are similar, which are 3.27–3.49, 3.39 and 3.02–3.19, respectively. The R_1 value of the Es_3^U at the slope location is 3.26. The R_1 values of the Es_3^M at the sag location are 1.74–2.68 (Figs. 20c; 21). The oil maturity of the Es_3^M at the sag location increases obviously with increasing depth.

Data from the above three methods show that the oil maturity of the Es_2, Es_3^U and Es_3^M at the high structural location and the Es_3^U at the slope location are similar and that oil maturity has no obvious correlation with depth. The oil maturity of the Es_3^M at the slope and sag locations increases obviously with increasing depth. Moreover, the oil maturity of the Es_3^M at the slope and sag locations is significantly higher than that of the Es_2, Es_3^U and Es_3^M at the high structural location and the Es_3^U at the slope location.

6.2. *Sandstone tightness history*

Previous studies indicate that five diagenetic stages occurred in the Dongpu Depression, including early-stage A, early-stage B, middle stage A_1, middle stageA_2 and middle stage B (Ji et al., 1992; Ji et al., 1995; Jiang et al., 2015). In early-stage A, the depth was <1800 m, and this stage included compaction. The depth of early-stage B was 1800–2800 m, and compaction and early cementation occurred, resulting in siderite, hematite, rhodochrosite, calcite, and gypsum. The depth of middle stage A_1 was 2800–3200 m, and compaction and dissolution occurred, resulting in dissolution of the secondary enlarged edge of quartz, early feldspar, debris, and carbonate cement. The depth of middle stage A_2 was 3200–3800 m, and compaction and cementation occurred, including cementation of secondary enlarged quartz edges, iron calcite, ankerite, and anhydrite. The depth of middle stage B was 3800–5000 m, and compaction occurred (Ji et al., 1992; Ji et al., 1995; Jiang et al., 2015).

Combining the burial history with the paleo porosity evolutionary model of the Es sandstone in the eastern Wenliu area (Eqs. 1–5), the porosity evolutionary history of sandstone in different structural loca-

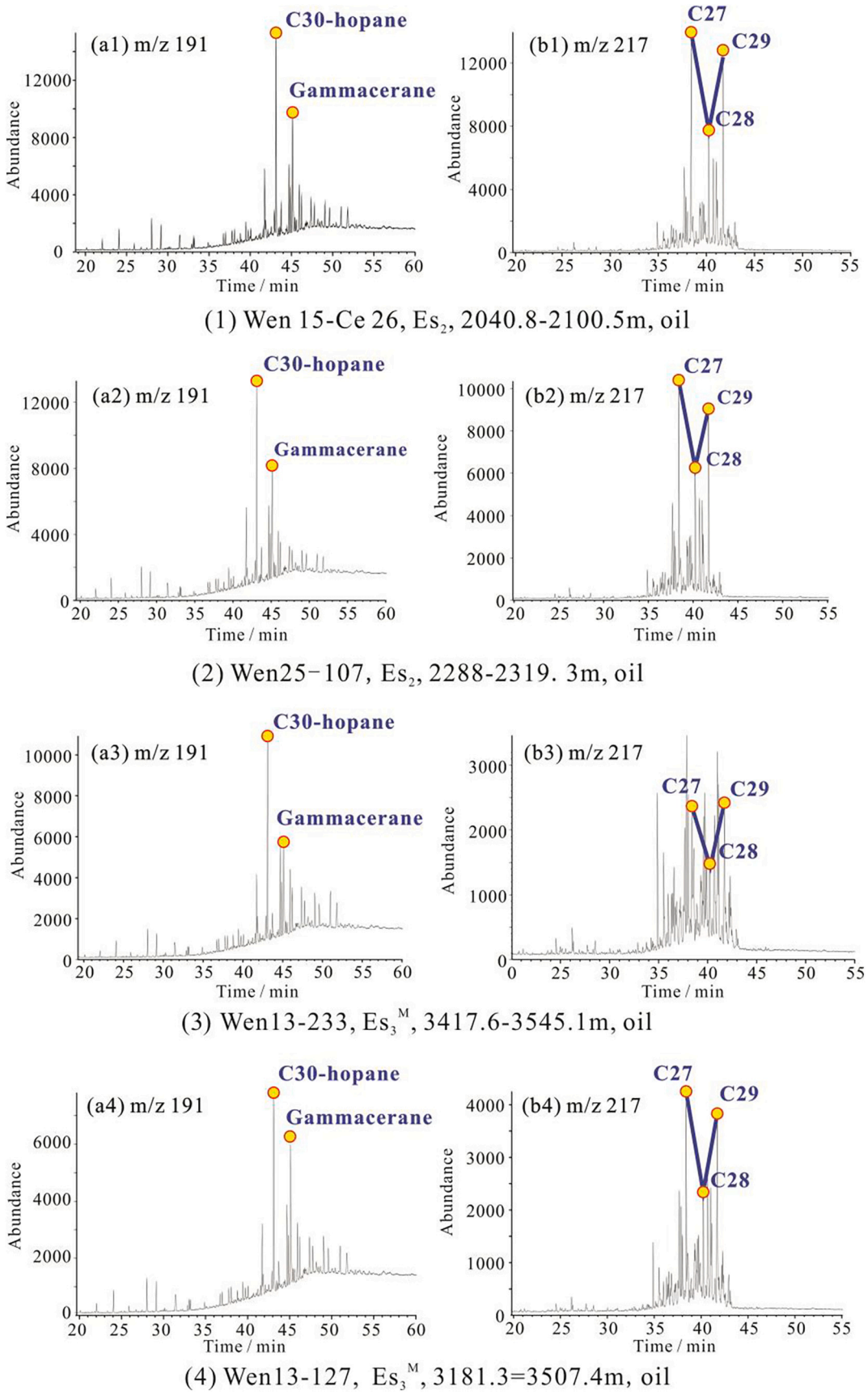

Fig. 14. Distribution characteristics of Terpane and Sterane of oil in structural high position in DCHA of eastern Wenliu areaeastern Wenliu area, Dongpu Depression.

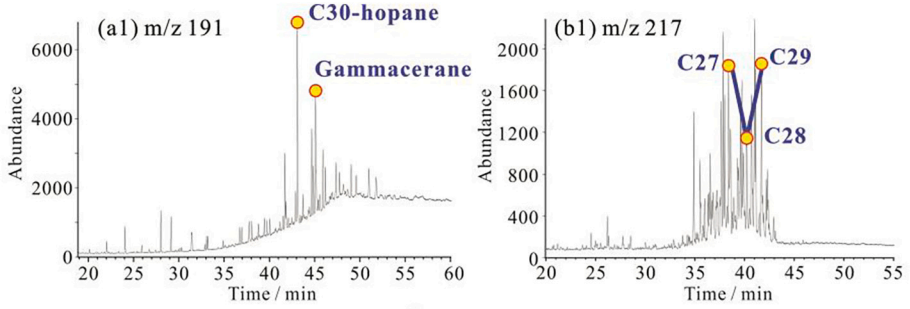

(1) Wen92-127, Es_3^U, 2928-3074m, oil

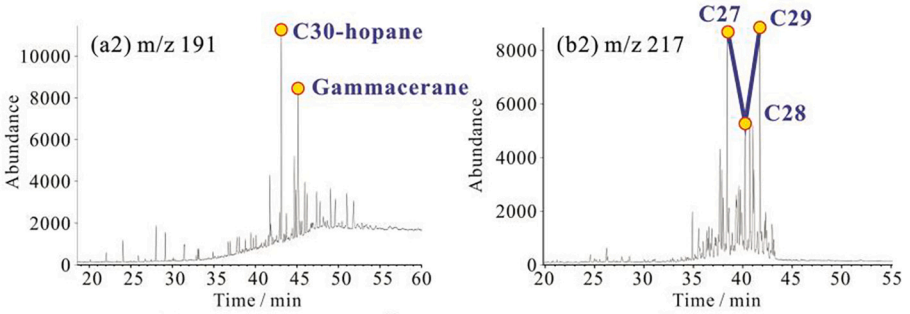

(2) Wen92−125, Es_3^U, 2902. 5-3181. 5m, oil

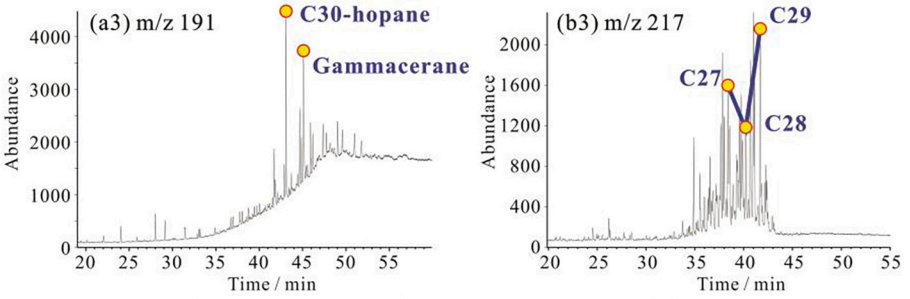

(3) Wen92-138, Es_3^M, 3510.1-3561.8m, oil

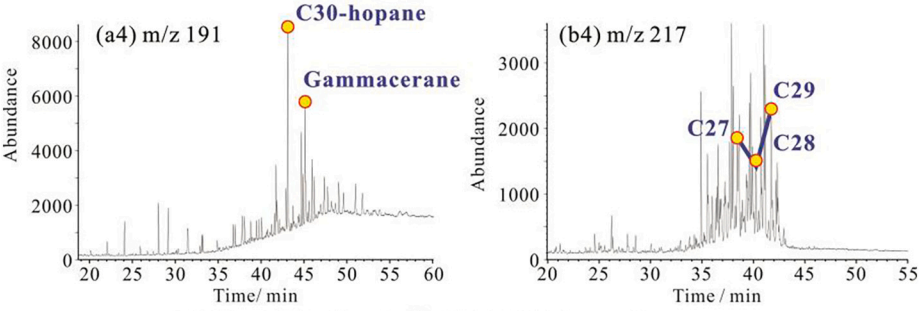

(4) Wen203−49, Es_3^M, 3508-3749m, oil

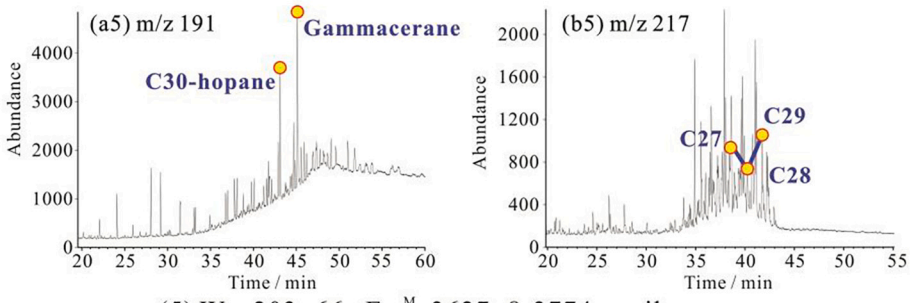

(5) Wen203−66, Es_3^M, 3627. 8-3774m, oil

Fig. 15. Distribution characteristics of Terpane and Sterane of oil in structural slope position in DCHA of eastern Wenliu areaeastern Wenliu area, Dongpu Depression.

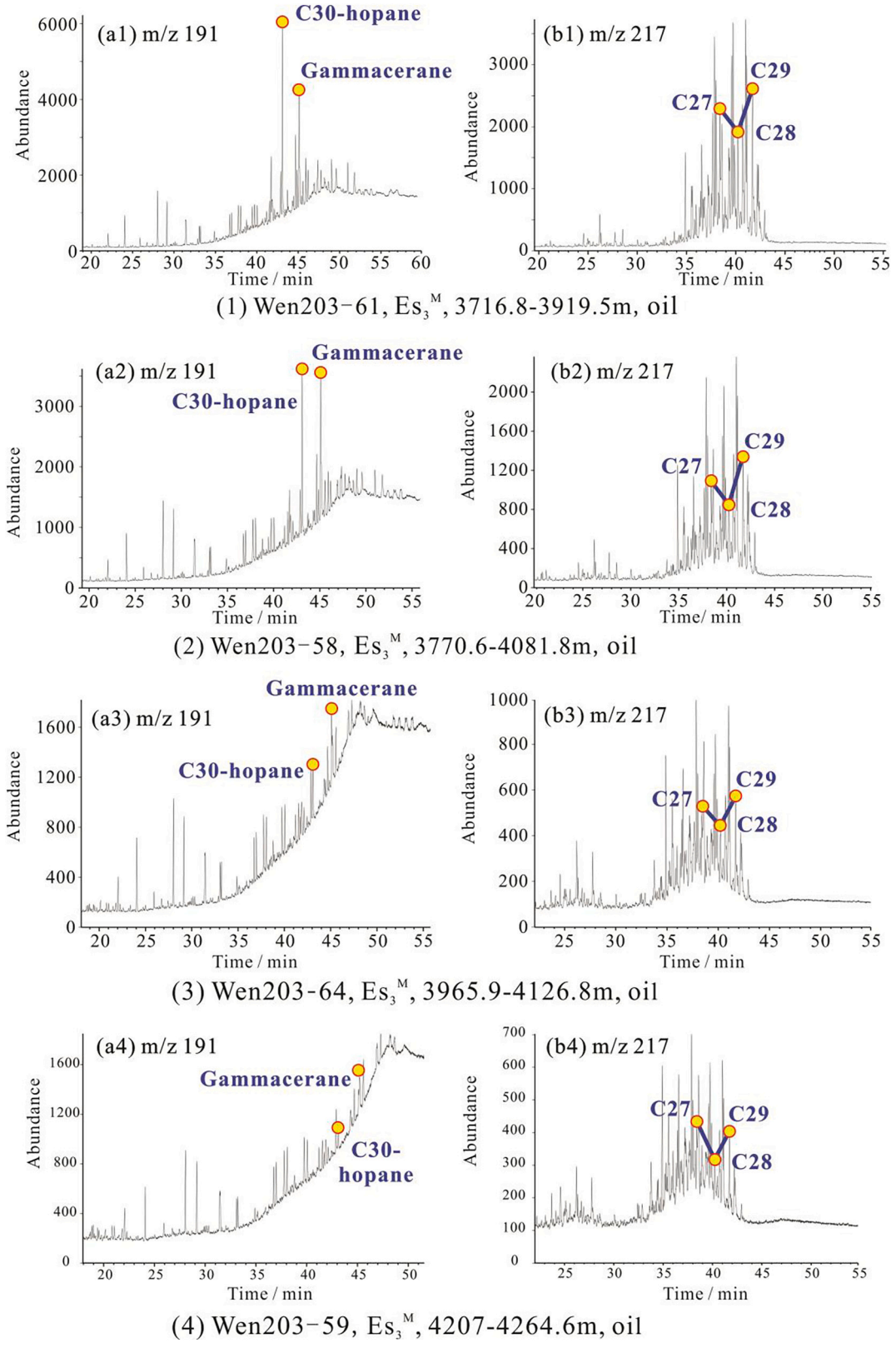

Fig. 16. Distribution characteristics of Terpane and Sterane of oil in structural sag position in DCHA of eastern Wenliu areaeastern Wenliu area, Dongpu Depression.

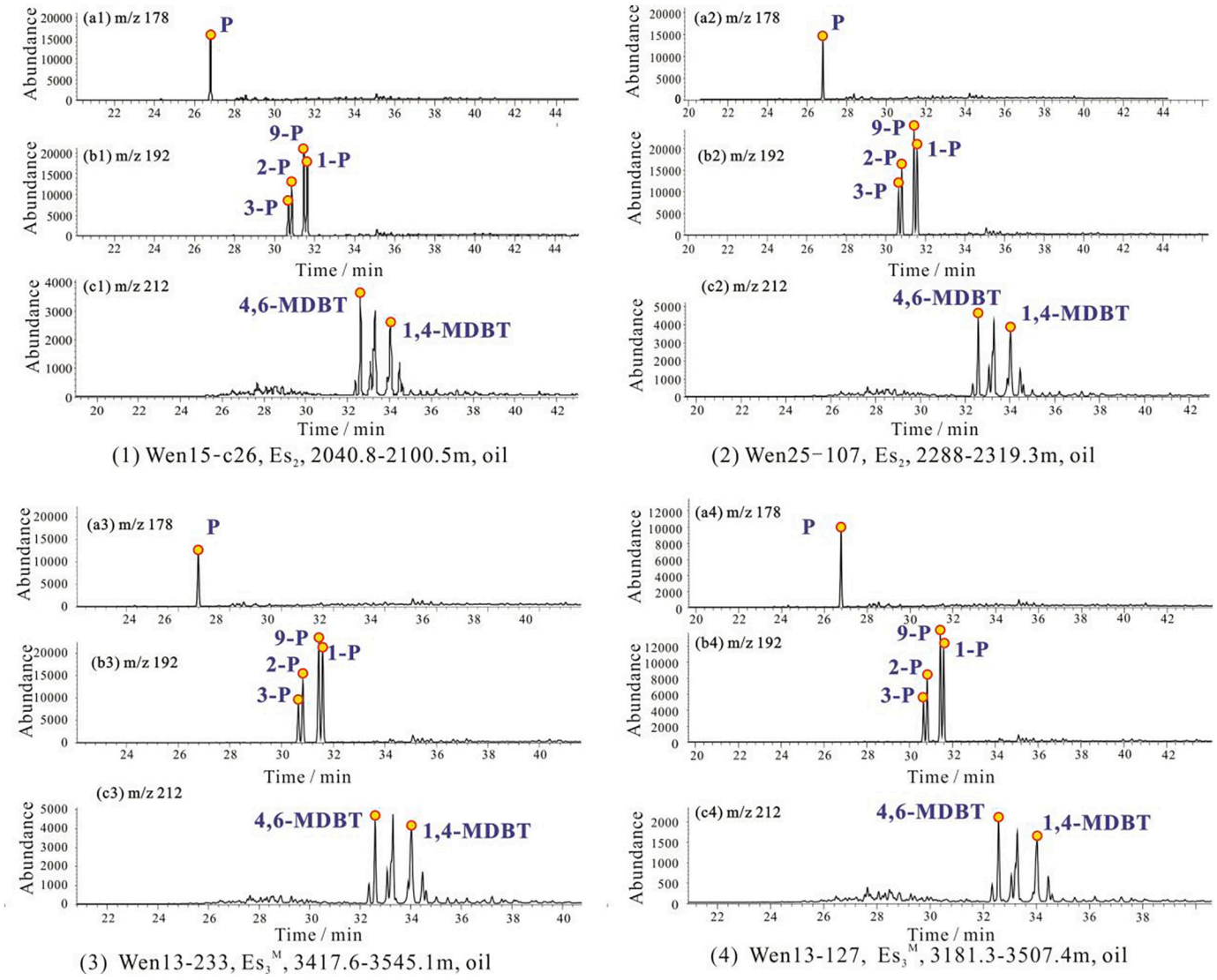

Fig. 17. Distribution characteristics of aromatics of oil in structural high position in DCHA of eastern Wenliu areaeastern Wenliu area, Dongpu Depression.

tions and strata was restored. To analyze the difference in the porosity evolution in sandstone in different structural locations and strata in the DCHA, three exploration wells located from the high structural location (Wen 15-Ce 26), slope (Wen 203–66) and sag (Qiancan 2) were selected to conduct basin modeling with PetroMod 1D. The lithology, rock thermal conductivity, stratigraphic age, sedimentation and denudation events, paleo-heat flow, paleo-surface temperature and paleo-water depth modeling data were obtained from Zuo et al. (2017), and the denudation thickness data were obtained from Lu et al. (2007).

$$\varphi = \varphi_0 \times e^{-cz} \quad z: 0\text{–}1800\ m \tag{1}$$

$$\varphi = \varphi_0 \times e^{-cz} - C_{AR} \times \frac{z-1800}{2800-1800} - C_m \times \frac{z-1800}{2800-1800} - C_Q \times \frac{z-1800}{3800-1800} \quad z: 1800\ m\text{–}2800\ m \tag{2}$$

$$\varphi = \varphi_0 \times e^{-cz} - C_{AR} - C_m - C_Q \times \frac{z-1800}{3800-1800} + C_d \times \frac{z-2800}{3200-2800} \quad z: 2800\ m\text{–}3200\ m \tag{3}$$

$$\varphi = \varphi_0 \times e^{-cz} - C_{AR} - C_m + C_d - C_Q \times \frac{z-1800}{3800-1800} - C_A \times \frac{z-3200}{3800-3200} \quad z: 3200\ m\text{–}3800\ m \tag{4}$$

$$\varphi = \varphi_0 \times e^{-cz} - C_{AR} - C_m + C_d - C_Q - C_A \quad z :> 3800\ m \tag{5}$$

where φ is the porosity (%) of the rock. φ_o is the initial porosity of the rock (%) at 35.91%. Z is the depth (m), C is the compaction factor (related to the particle size of the rock) at 0.00033. C_{AR} is the content of early cements in rocks, and the values of the Es_3^L, Es_3^M, and Es_3^U sandstones are 10.78%, 4.67% and 14.62%, respectively. C_m is the porosity decrease caused by the cementation of iron and manganese minerals, and the values of the Es_3^L, Es_3^M, and Es_3^U sandstones are 0.68%, 0.63% and 1.43%, respectively. C_Q is the porosity decrease caused by the secondary enlargement of quartz and the content of authigenic quartz; the values of the Es_3^L, Es_3^M, and Es_3^U sandstones are 0.67%, 0.30% and 0.04%, respectively. C_d is the secondary porosity increase caused by the dissolution of grains and cements in rocks, and the values of the Es_3^L, Es_3^M, and Es_3^U sandstones are 2.13%, 2.17% and 2.29%, respectively. C_A is the porosity change caused by cement in the middle-late stage diagenesis, and the values of the Es_3^L, Es_3^M, and Es_3^U sandstones are 25.30%, 20.58% and

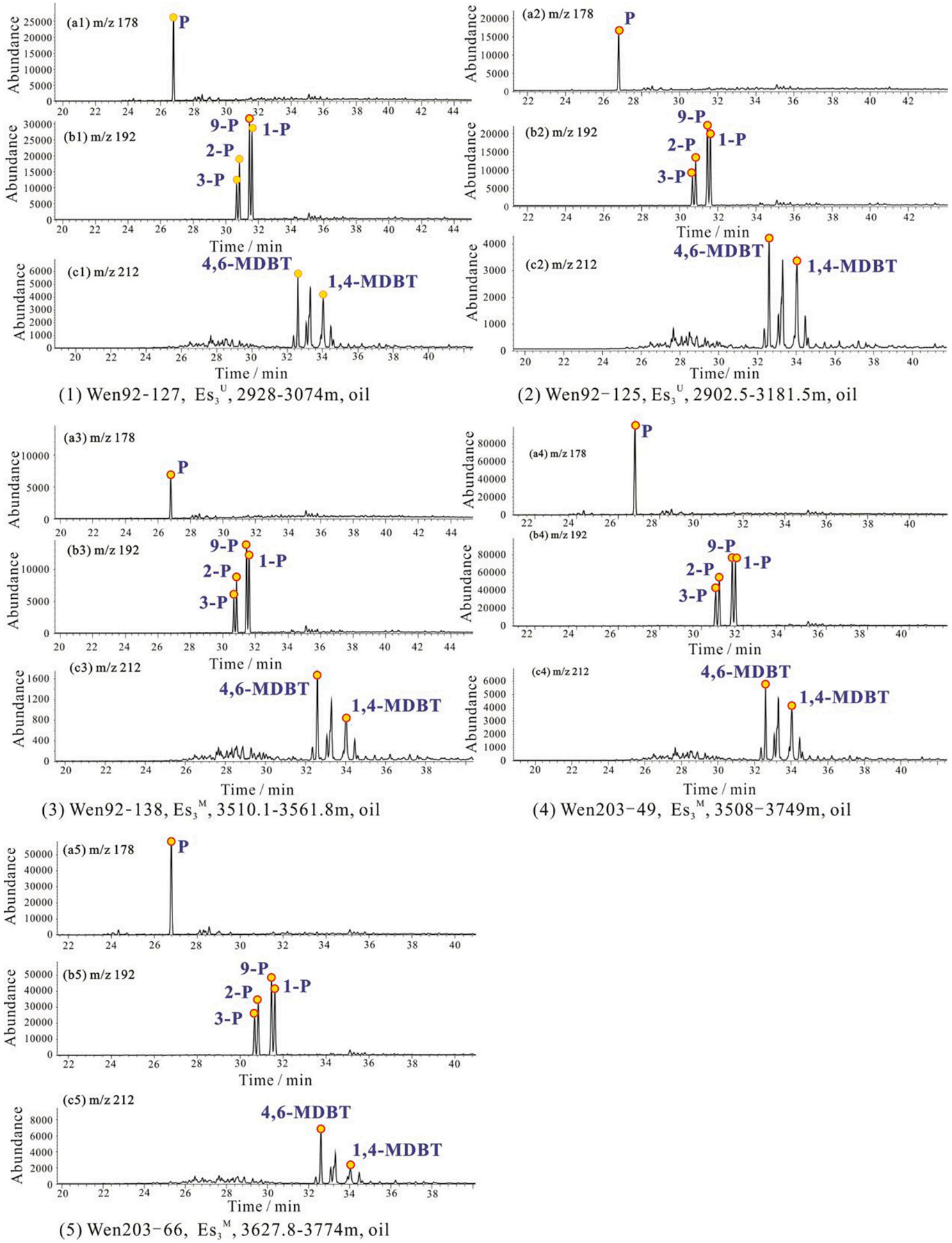

Fig. 18. Distribution characteristics of aromatics of oil in structural slope position in DCHA of eastern Wenliu areaeastern Wenliu area, Dongpu Depression.

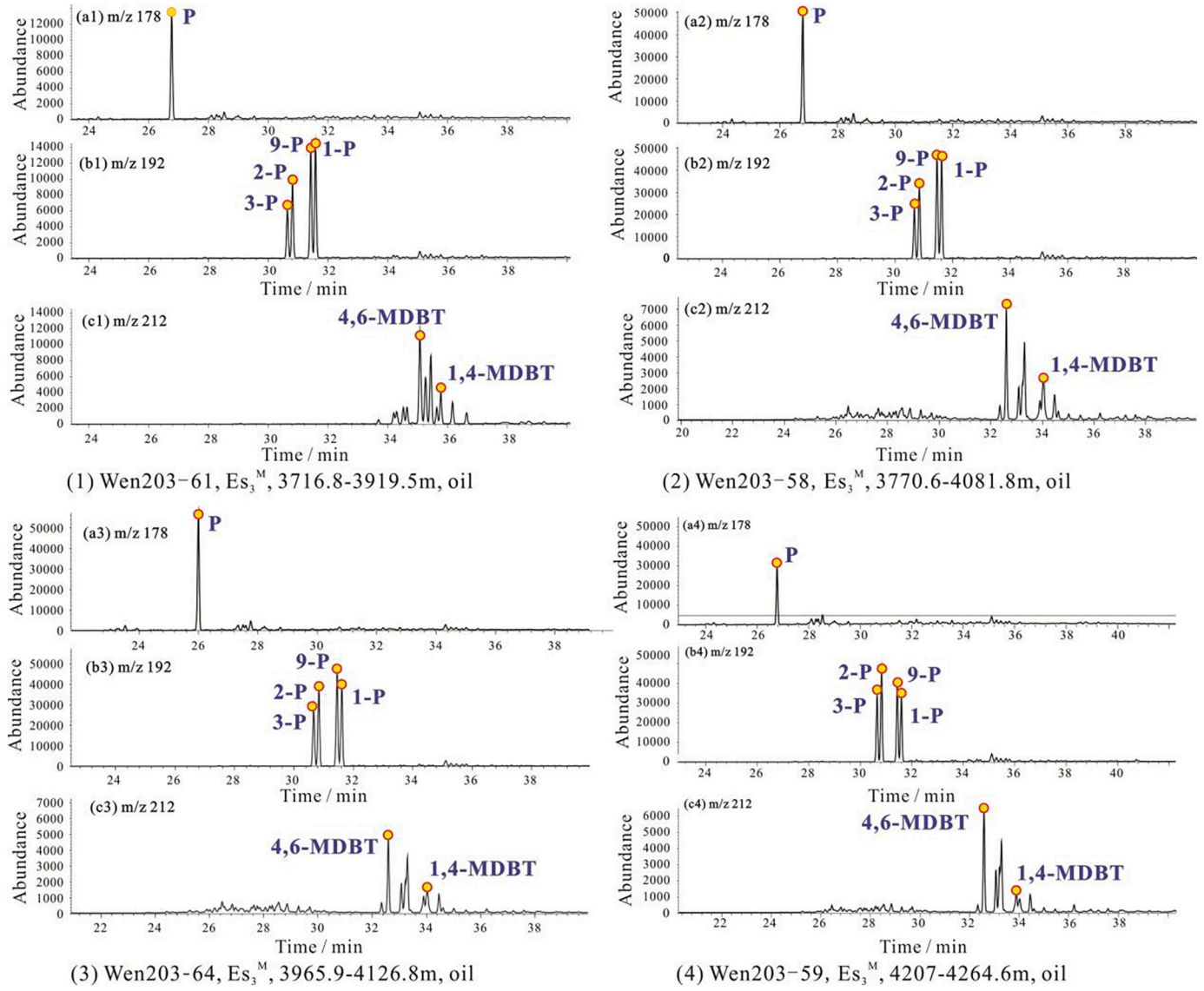

Fig. 19. Distribution characteristics of aromatics of oil in structural sag position in DCHA of eastern Wenliu areaeastern Wenliu area, Dongpu Depression.

20.95%, respectively.

In the Es_3^U sandstone reservoir, the porosities in the structural high, slope, and sag locations were >10% at the end of the Ed sedimentation period and remain that way today (Fig. 23a). In the Es_3^M sandstone reservoir, the porosities in the slope and sag locations were >10% at the end of the Ed sedimentation period, while they were <10% in the late Nm sedimentation stage (2.2 Ma and 1.5 Ma) (Fig. 23b). In the Es_3^L sandstone reservoir, the porosity in the sag location was <10% in the middle Ed sedimentation period (28.5 Ma). Then, although the porosity was >10% again due to the influence of strata uplift and dissolution diageneses, the strata continued to subside later, and the current porosity was approximately 7% (Fig. 23c).

Because the burial depth of Es_2 is less than that of Es_3^U and the depth of Es_4^U is greater than that of Es_3^L, the following conclusions can be drawn: 1) the porosities of the Es_3^U and Es_2 sandstones in the structural high, slope and sag locations were >10% at the end of the Ed sedimentation period and have remained so until the present; 2) the porosity of the Es_3^M sandstone at the slope location was >10% at the end of the Ed sedimentation period, and it is now <10% as a whole; 3) the porosity of the Es_3^M sandstone near the sag was >10% in the late Ed sedimentation period, and it is currently <10% overall; 4) the porosity of the Es_3^L sandstone near the sag was <10% at 28.5 Ma (middle Ed sedimentation period); and 5) the porosity of the Es_4^U sandstone near the sag was <10% in the early-middle Ed sedimentation period.

6.3. Formation of hydrocarbon inclusions and petroleum charging times

As the thermal maturity increases, the fluorescence color of hydrocarbon inclusions evolves toward blue, i.e., from brown to yellow, yellow-white, yellow-green, blue-white, and finally blue (George et al., 2002; Munz, 2001). For the twenty sandstone cores studied, the fluorescence colors of the hydrocarbon inclusions display distinct differences in the type and time of petroleum charging at different structural locations and in different strata. For the high structural location, the Es_2 and Es_3^U petroleum at the shallow location comes from mature source rocks, and the Es_3^M petroleum at the deep location comes from mixed mature and highly mature source rocks. For the slope location, the Es_3^U petroleum originated from mixed mature and highly mature source rocks, and the Es_3^M petroleum came from highly mature source rocks. At the sag location, all the Es_3^M and Es_3^L petroleum came from highly mature source rocks.

The formation time of hydrocarbon inclusions depends on the host minerals and associated distribution of hydrocarbon inclusions in the fractures, the reservoir burial history, and the diagenetic evolution

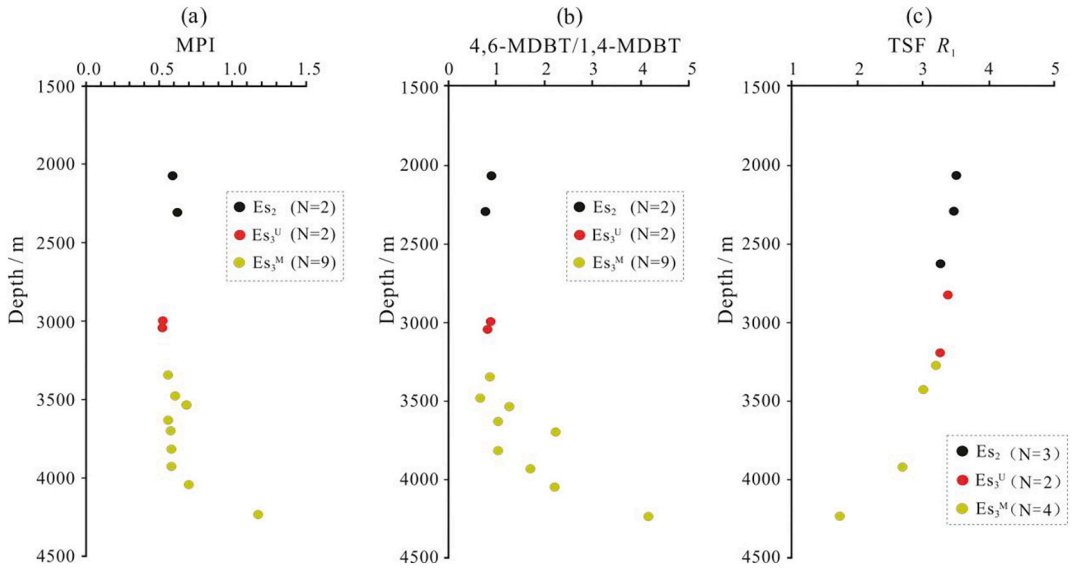

Fig. 20. Correlation between thermal maturity indices of oil and depth in DCHA of eastern Wenliu areaeastern Wenliu area, Dongpu Depression.

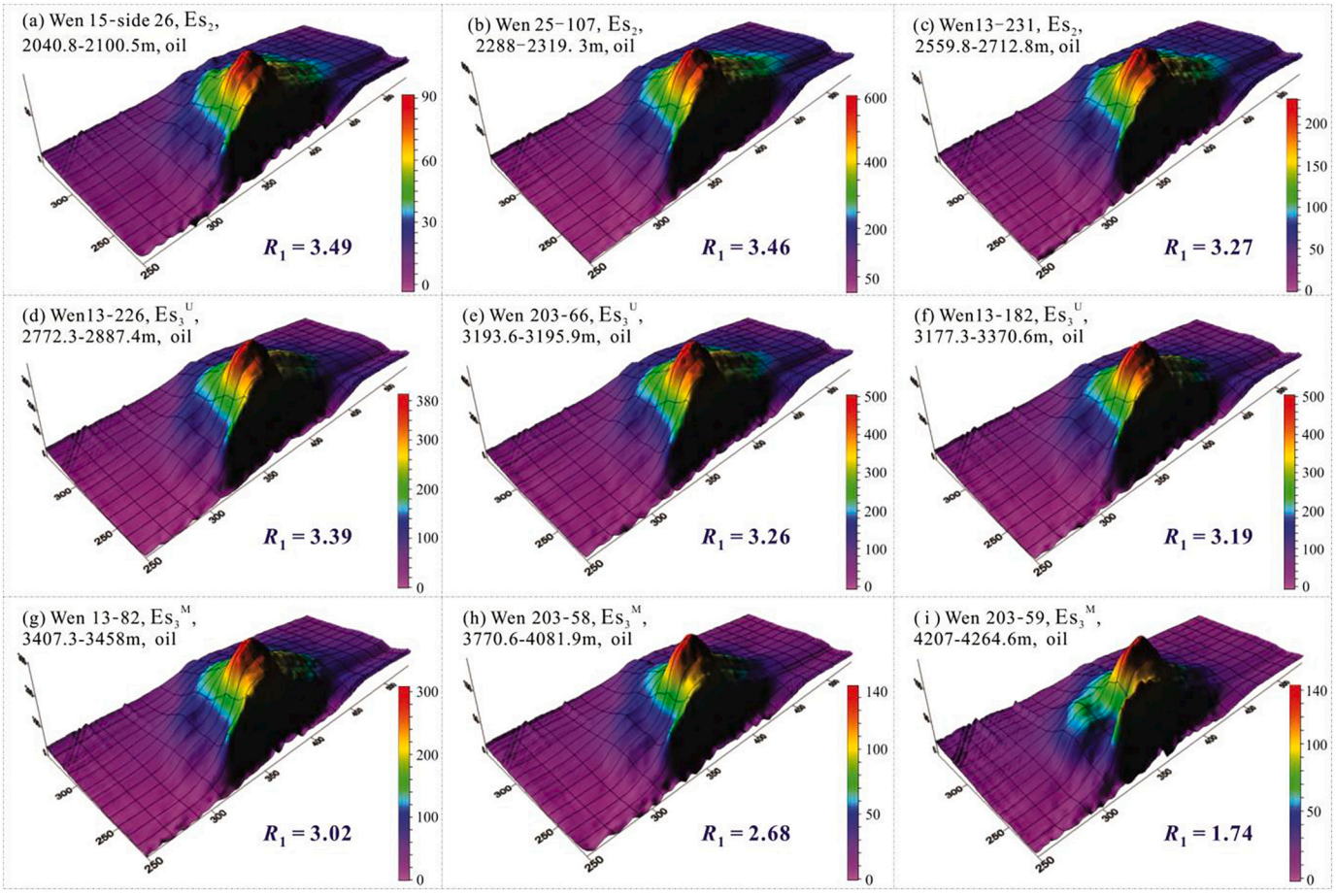

Fig. 21. Total Scanning Fluorescence (TSF) of oil in DCHA of eastern Wenliu areaeastern Wenliu area, Dongpu Depression.

sequence (Jiang et al., 2015; Liu et al., 2013; Tao, 2006). The examination of twenty sandstone cores shows that the hydrocarbon fluid inclusions occur in the secondary enlarged margins of quartz, intracrystalline dissolved pores of feldspar, intracrystalline dissolved pores of quartz, and intragranular fractures in quartz and quartz cracks (Figs. 8–12).

Combined with the previously established diagenetic evolutionary sequence (Ji et al., 1992; Ji et al., 1995; Jiang et al., 2015), it was determined that the secondary enlarged margins of quartz formed in early diagenetic stage B and the intracrystalline dissolved pores of feldspar and quartz were formed in late diagenetic stages A_1 and A_2, and the intragranular fractures in quartz began to form in middle diagenetic

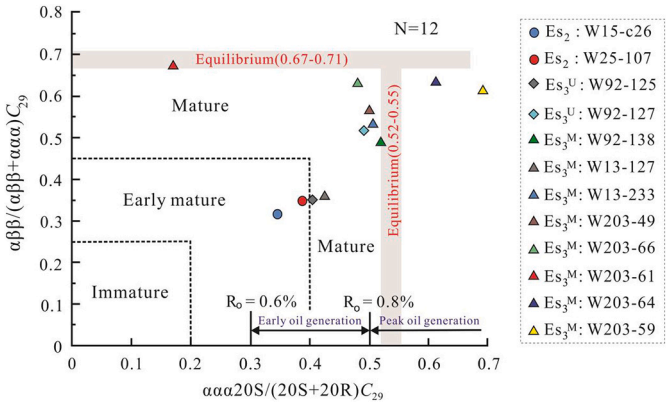

Fig. 22. Representative maturity biomarker indices of oil in DCHA of eastern Wenliu areaeastern Wenliu area, Dongpu Depression.

stage A_1. Due to the intense tectonic movement in the late Paleogene, the stress field of the formation fluctuated dramatically, leading to the formation of abundant microfractures (intragranular fractures in quartz and quartz cracks), which could capture petroleum to form inclusions during the healing process in later subsidence.

Based on the above analyses and reservoir burial evolutionary history (Jiang et al., 2015; Zhang et al., 2016), hydrocarbon inclusions formed in two stages: 1) the early stage, i.e., the middle-late Ed sedimentation stage to early uplift stage, in intracrystalline dissolved pores of feldspar and quartz, secondary enlargement of quartz, and intragranular fractures of quartz, and 2) late stage, i.e., the late Minghuazhen Formation (Nm) sedimentation stage to present, as clustered and bead-like inclusions in intragranular fractures in quartz, which caused quartz cracks to form.

The petroleum charging time was determined based on the hydrocarbon inclusions and their petrographic features, the measured HTBI homogenization temperatures, and the thermal evolutionary history. For the high structural location, the HTBIs associated with the yellow hydrocarbon inclusions in the Es_2 sandstone (Wen 25–23) at the shallow location are 72 °C–86 °C, and combined with the thermal evolutionary history of the Es_2, the petroleum charging time occurred from 27.2 Ma to 23.1 Ma (Fig. 24a). Similarly, the petroleum charging time of the Es_3^U sandstone (Wen 15–14) at the shallow location was 26.8 Ma–22.8 Ma (Fig. 24b), the charging times of the deep Es_3^M sandstone (Wen 13–281) were 26.2 Ma–23.1 Ma and 2.2 Ma–0 Ma (Fig. 24c), and the charging times of the Es_3^M sandstone (Wen 13–110) were 26.4 Ma–22.8 Ma and 2.3 Ma–0 Ma (Fig. 24d). For the slope location, the petroleum charging times of the Es_3^U sandstone (Wen 92–56) were 27.0 Ma–22.7 Ma and 3.1 Ma–1.5 Ma (Fig. 25a), and the charging time of in Es_3^M sandstone (Wen 203–35) was 3.1 Ma–0 Ma (Fig. 25b). For the sag location, the petroleum charging time of the Es_3^M sandstone reservoir (Wen 203–59) was 4.2 Ma–0 Ma (Fig. 26a), and the charging time of the Es_3^L sandstone (Pushen 7) was 2.8 Ma–0 Ma (Fig. 26b).

Corresponding to the two stages of formation of hydrocarbon inclusions, the DCHA of the Es in the Dongpu Depression underwent two petroleum charging times, i.e., the middle-late Ed sedimentation stage to the early uplift stage (27.2 Ma–22.7 Ma) and the middle-late Nm sedimentation stage to present (4.2 Ma–0 Ma). However, there were differences in petroleum charging times at different structural locations and strata. For the high structural location, only early mature petroleum charging occurred in the Es_2 and Es_3^U sandstones at the shallow strata, and two petroleum charging times (early mature petroleum and late highly mature petroleum) occurred in the Es_3^M sandstone at the deep strata. For the slope location, two petroleum charging times occurred in the Es_3^U sandstone, while only highly mature petroleum charging occurred in the Es_3^M sandstone. At the sag location, only highly mature petroleum charging occurred in the Es_3^M and Es_3^L sandstones.

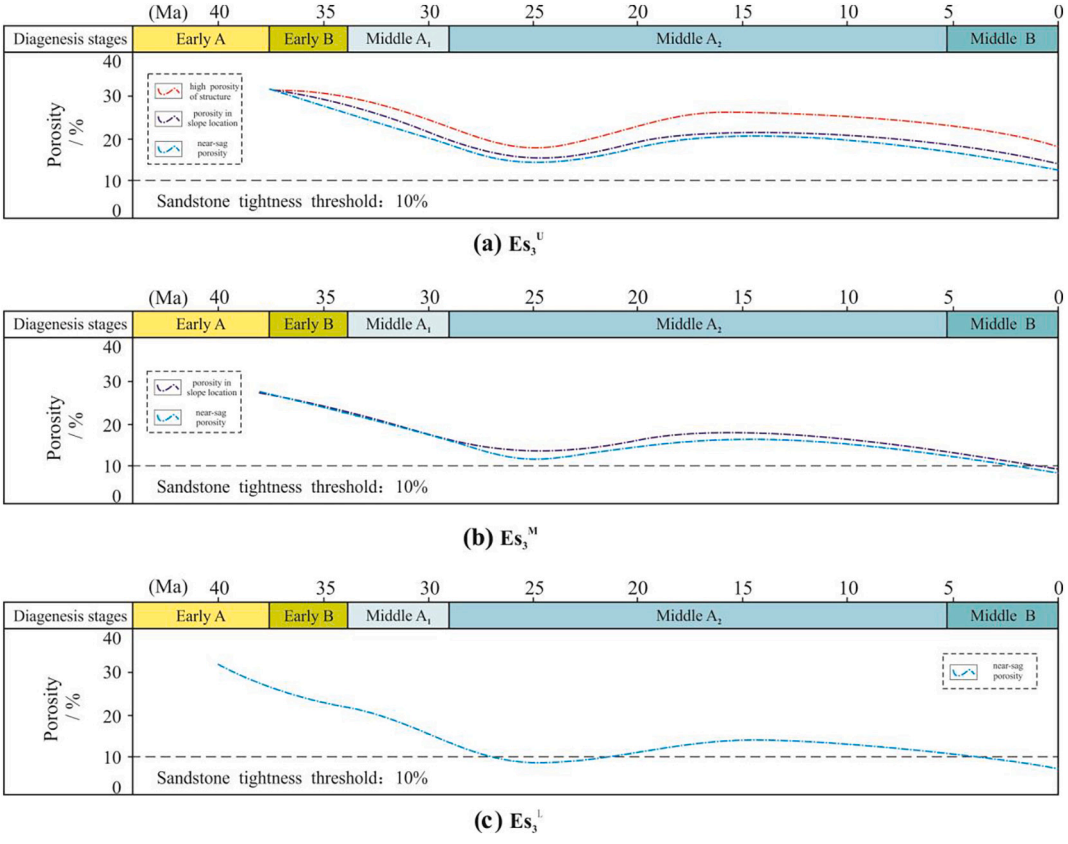

Fig. 23. Porosity evolution in different Es sandstones in DCHA of eastern Wenliu areaeastern Wenliu area, Dongpu Depression.

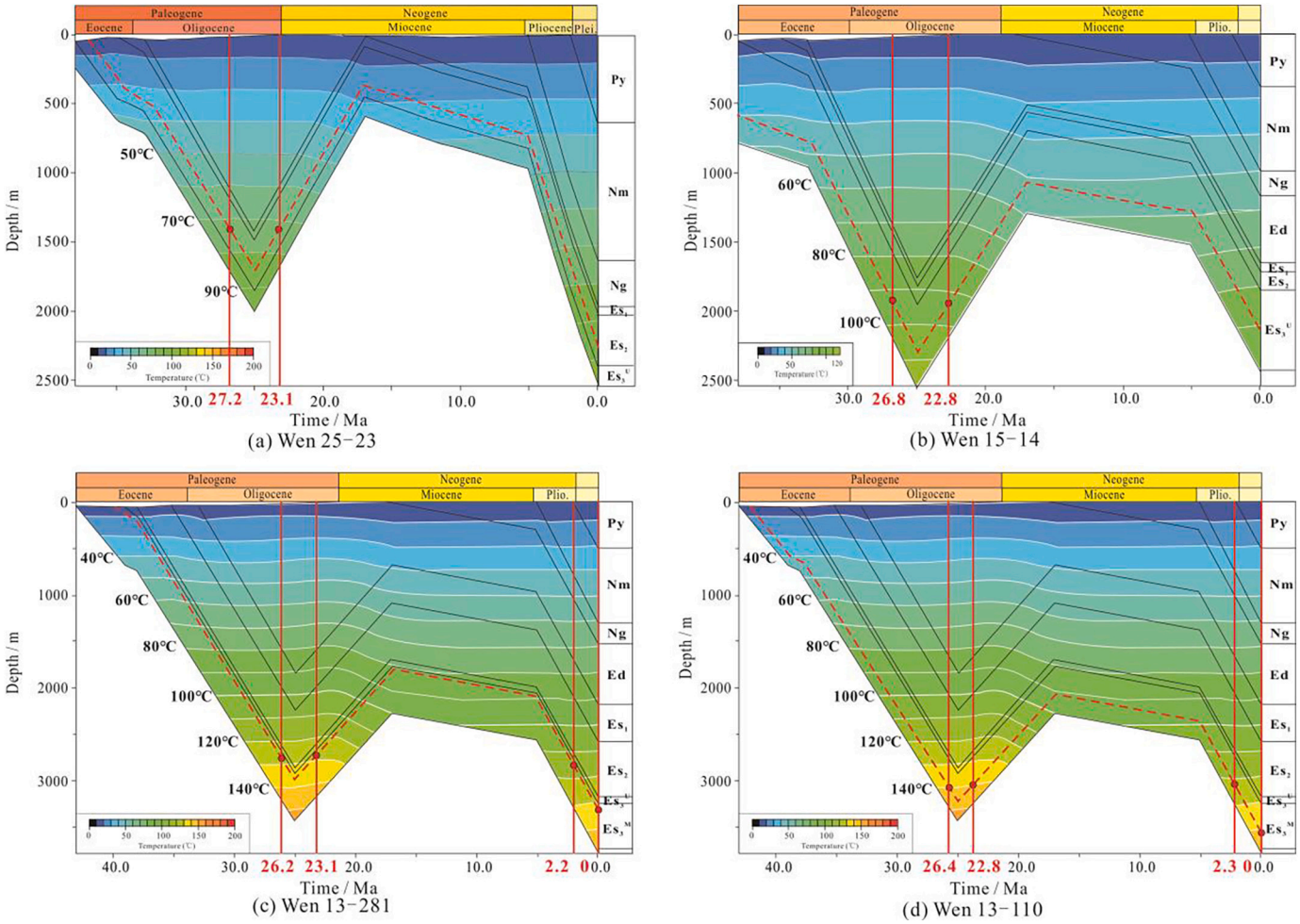

Fig. 24. Petroleum charging times in Es in structural high position in DCHA of eastern Wenliu area, Dongpu Depression.

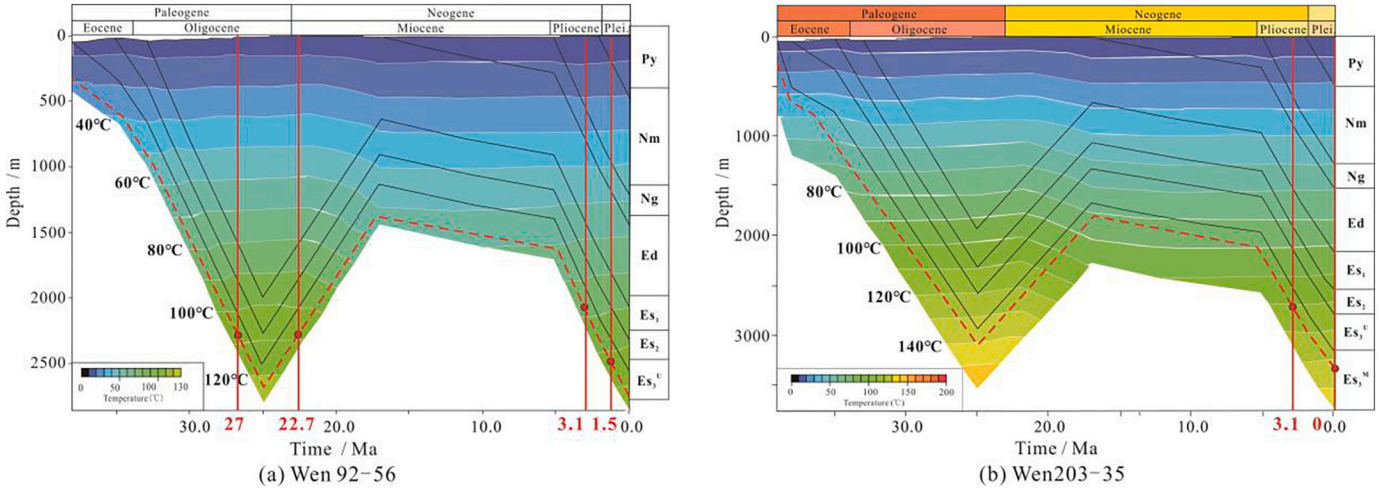

Fig. 25. Petroleum charging times in Es in structural slope position in DCHA of eastern Wenliu area, Dongpu Depression.

Jiang et al., 2015 and Zhang et al. (2016) also indicated that there were two petroleum charging times in the Es of the Dongpu Depression, i.e., the middle-late Ed sedimentation stage to the early uplift stage and the late Nm sedimentation stage to the present. However, they believed that the early petroleum charging was extensive and distributed throughout the Dongpu Depression, and the late petroleum charging was distributed near the sag, which is different from our study. We found that early petroleum charging occurred at the structural high and slope locations, especially at the high location, and late petroleum charging mainly occurred at the sag and slope locations, especially at the sag. In other words, one petroleum charging time occurred in the structural high and sag locations, while two petroleum charging times occurred in

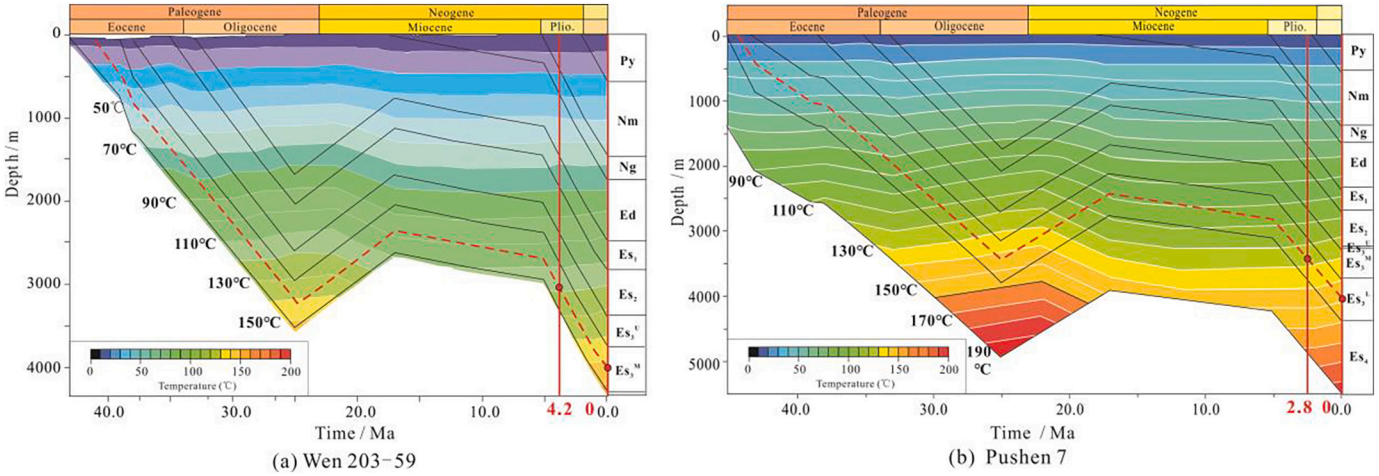

Fig. 26. Petroleum charging times in Es in structural sag position in DCHA of eastern Wenliu area, Dongpu Depression.

the structural slope location. Moreover, the onset time for late petroleum charging at the sag is earlier than that at the slope. For the high structural location, the petroleum charging time is the earliest. For the slope location, the petroleum charging time of the Es_3^U sandstone is earlier, while that of the Es_3^M is late. For the sag location, the petroleum charging time of the Es_3^M is the latest.

6.4. Petroleum charging forces

6.4.1. Critical porosity threshold and dynamic petroleum charging processes

Previous studies of petroleum accumulation conditions of DCHAs (Jia et al., 2012; Liu et al., 2014a, 2014b, 2014c; Ma, 2008; Zou et al., 2009a, 2009b), reservoir physical property statistics (Duan et al., 2008; Jia et al., 2012; Liu et al., 2014a, 2014b, 2014c; Zou et al., 2009a, 2009b), physical simulation experiments (Gies, 1984; Jia et al., 2012; Pang et al., 2003) and numerical simulation experiments (Guo, 2013; Ma, 2008; Pang et al., 2012; Cai et al., 2021) have revealed that there is a critical porosity threshold for dynamic petroleum charging processes. Pang et al. (2014a, 2014b, 2021a) calls it the buoyancy-driven hydrocarbon accumulation depth (BHAD), which is the limit of buoyancy action (Pang et al., 2014b; Pang et al., 2021; Pang et al., 2014b; Pang et al., 2003). Above the BHAD, buoyancy is the key driving force for petroleum migration, and the accumulated petroleum reservoirs have "four highs", i.e., petroleum accumulated in the high points of traps, enriched in layers with high porosity and permeability, distributed in high locations sealed by caprocks, and formed with high fluid pressure in reservoirs (Pang et al., 2021). Below the BHAD, petroleum migration and accumulation are dominated by non-buoyancy forces, such as capillary force and overpressure, in tight reservoirs with "four lows", i.e., petroleum is distributed in the low basin depressions, accumulates in layers with low porosity, is located in the form of inverted low locations, and is stable at low pressures (Pang et al., 2021).

Studies of the porosity surrounding the BHAD revealed that the critical porosity values at the BHAD are 10%–12% (Jia et al., 2012; Pang et al., 2012; Pang et al., 2021a; Pang et al., 2021b; Zou et al., 2009a, 2009b). Based on the "force balance" at the BHAD, Guo et al. (2017) simulated numerically the critical porosity threshold of the BHAD and confirmed it to be 10% (Guo, 2013; Guo et al., 2017). The significance of the critical porosity threshold of the BHAD is that when the porosity of the Es sandstone in the Dongpu Depression is >10%, the key petroleum charging force is buoyancy and petroleum migrates into the reservoir via a "displacement mode", that is, oil and natural gas moves upward in bubbles or columns driven by buoyancy in water, resulting in gas-water position exchange) (Jin and Zhang et al., 2003; Zhang et al., 2008), and the accumulated petroleum reservoir thus contains a normal oil-gas-water interface (gas at the top, oil at the middle, and water at the bottom). And when the porosity of the Es sandstone is <10%, the petroleum charging force is nonbuoyant, and petroleum mainly migrates into the reservoir via a "piston mode" under overpressure and forms inverted oil-gas-water interfaces, i.e., an inverted oil-water interface (water at the top and oil at the bottom), inverted oil-gas interface (oil at the top and gas at the bottom), and no gas-water interface. During the migration, if the petroleum source is completely depleted due to diffusion, the tight petroleum range will shrink gradually (Guo, 2013; Guo et al., 2017; Jiang et al., 2006; Liu et al., 2014a, 2014b, 2014c; Ma, 2008; Pang et al., 2012; Pang et al., 2014b).

6.4.2. Pressurization due to petroleum generation

As described in Section 5.1, Es_2 and Es_3^U in the DCHA in the high structural location in the Dongpu Depression have normal to weak overpressure, and Es_3^M in the slope and sag locations have normal to strong overpressure. Previous studies have shown that formation overpressure is mainly caused by undercompaction and petroleum generation or a combination of the two (Bourgoyne, 1990; Hao, 2005; Hunt, 1990; Osborne and Swarbrick, 1997; Zhao et al., 2017), in which undercompaction generally occurs in thick shale that is buried rapidly and continuously. The Es in the eastern Wenliu area is characterized by thin interbedded development of sandstone and shale, and a single layer of shale is thin (<20 m, with a mean of 5–11 m). Moreover, the sedimentation rate of the Es is low (Liang et al., 2017a,b); thus, undercompaction is not the key factor inducing overpressure. The eastern Wenliu area is close to the Qianliyuan Sag, which is the best area for petroleum generation with the greatest petroleum generation quantity and the highest thermal maturity in the Dongpu Depression. The depth at which the petroleum generation in Es_3 peaked, corresponding well to the depth range of overpressure (Liang et al., 2017a, 2017b; Liu and Liu, 2018; Wang et al., 2018), indicating that the overpressure is mainly caused by the pressurization of petroleum generation. Vertically, overpressure existed in the Es_3 at the slope location. In the horizontal direction, overpressure caused pressurization of petroleum generation increases from the structural high to the slope and to the sag locations (Liu and Liu, 2018).

6.4.3. Buoyancy and overpressure as petroleum charging forces

According to the petroleum charging times (Section 6.5), the sandstone tightness history (Section 6.2), and formation overpressure, petroleum charging dynamics at different structural locations and in different strata in the DCHA were determined.

During the middle-late sedimentation and early uplift of the Ed, all the Es_2, Es_3^U, and Es_3^M sandstone porosities at the structural high location and the Es_3^U porosity at the slope location were >10% (conventional).

Under buoyancy, petroleum originating from the sag center accumulated first in the Es_2 sandstone reservoir at the high structural location via a "displacement mode" (Pang et al., 2021a, 2021b). After the Es_2 reservoir was filled with petroleum, migrated petroleum subsequently accumulated in the Es_3^U sandstone reservoir in a "displacement mode" at the structural high and slope locations under buoyancy (Pang et al., 2021a, 2021b). When petroleum was replenished continuously, petroleum subsequently migrated and accumulated in the Es_3^M sandstone reservoir in a "displacement mode" at the high structural location under buoyancy.

During the middle-late Nm sedimentation stage to present-day, both the Es_3^M and Es_3^L sandstone porosities at the structural slope and sag locations were <10% (tight). Under the overpressure induced by petroleum generation pressurization, petroleum originating from the sag center accumulated first in the Es_3^M sandstone reservoir at the structural sag location in the "piston mode". As petroleum charging continues, when the Es_3^M sandstone reservoir at the sag location is full of petroleum, petroleum will continue to accumulate in the Es_3^M sandstone reservoir at the slope location in the "piston mode" under petroleum generation pressurization, gradually promoting petroleum distribution from the sag to the slope locations. With further petroleum charging, the tight sandstone reservoir in the Es_3^M at the slope will be full of petroleum, and when the petroleum charging range reaches the boundary of the tight sandstone reservoir (the critical porosity threshold 10%), charging forces will change from overpressure to buoyancy, and charging modes will change from "piston mode" to "displacement mode" simultaneously; thus, petroleum will accumulate in the Es_3^M sandstone reservoir at a high structural location.

In the high structural location, petroleum charging forces in Es_2, Es_3^U, and Es_3^M are buoyant. In the slope location, the charging force in Es_3^U is buoyancy, while that in Es_3^M is overpressure induced by petroleum generation pressurization. In the sag location, the charging force in Es_3^M is dominated by overpressure.

6.5. Petroleum charging stages

Faults and gypsum layers have important effects on petroleum migration and preservation in the Dongpu Depression (Jiang et al., 2015). Three gypsum layers developed in Es_3^L, middle-upper Es_3^M, and Es_1, and recently discovered petroleum resources are distributed under these gypsum layers (Du et al., 2008; Liu et al., 2014a, 2014b, 2014c; Qi et al., 1992). Faults are distributed in the high structural location, with less development in slope and sag locations (Cheng et al., 2015; Guo, 2014; Jiang and Cha, 2005; Pang et al., 2014b). Combined with the petroleum source, charging time, charging forces, reservoir tightness history, and structural background, the formation process of the DCHA occurred in four stages.

Fault movement in the Paleogene strata in the Dongpu Depression began during the Es_4 sedimentation period (Tang and Wang, 2008). A thick gypsum layer developed during Es_3^L sedimentation. The first main fault, the Wendong No.3 Fault, developed during the early Es_3^M sedimentation period. During late Es_3^M to Es_3^U sedimentation periods, fault activity became stronger and formed the present structural pattern of "two Sags, one Uplift and one Slope" in the Dongpu Depression, and a thick gypsum layer was deposited in Es_3^M at the same time. During the Es_3^U sedimentation period, shales in the Es in the sag did not yet generate

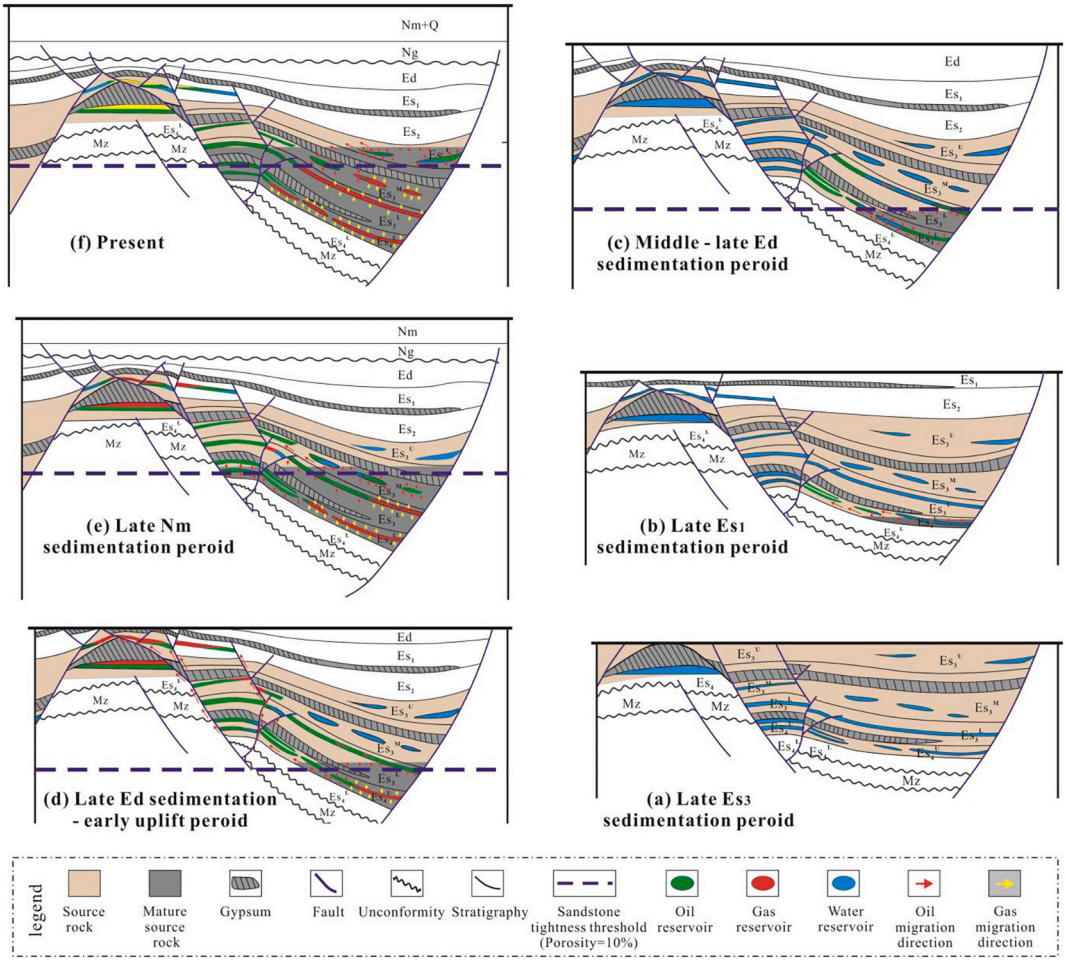

Fig. 27. Accumulation model of the DCHA of eastern Wenliu area, Dongpu Depression.

petroleum (Fig. 27a). During the early Es_2 sedimentation period, fault activity was strong, and the second main fault, the Xulou Fault, formed, but it had little influence on the structural pattern of the Dongpu Depression. At this time, shales in Es_4 in the sag center had entered the stage of low-maturity oil generation, while the oil generation amount was limited and did not reach the petroleum expulsion threshold.

1) **$Es_1$to early-middle Ed sedimentation stage: conventional petroleum accumulation at a high structural location beneath the gypsum layer under buoyancy with a distal petroleum source**. During the Es_1 sedimentation stage, the Es_4^U shales entered the mature oil generation stage (34.5 Ma) and began to expel petroleum. Es_3^L shales entered the mature oil generation stage in the early-middle Ed sedimentation period (30.7 Ma) and began to expel petroleum. Fault activity was weak at this time (Shi et al., 2007; Tang and Wang, 2008). Due to the thick gypsum layer developed in the Es_3^L and Es_3^M, faults could not cut through gypsum layers. Moreover, the Es_4^U and Es_3^L sandstone reservoirs were not tight yet, and thus petroleum generated from the Es_4^U and Es_3^L shales accumulated beneath the Es_4^U gypsum layers in the "displacement mode" under buoyancy (Fig. 27b), forming conventional petroleum reservoirs.
2) **Middle-late Ed sedimentation stage: superposition by tight petroleum at the sag and slope under the petroleum generation expansion force with a proximal petroleum source, conventional petroleum at a high location beneath the gypsum layer under buoyancy with a distal petroleum source, and in the initial formation stage of the DCHA.** During the middle-late Ed sedimentation period (27.8 Ma), fault activity was weak (Jiang et al., 2015; Shi et al., 2007; Tang and Wang, 2008). The Es_4^U shales entered the mature oil and gas generation stage, the Es_3^L shales entered the mature oil generation stage, the Es_3^M shales had entered the low-maturity oil generation stage and petroleum expulsion had not yet started. The Es_4^U and Es_3^L sandstone reservoirs were tight at this time; thus, petroleum generated from the Es_4^U and Es_3^L shales accumulated at the sag and slope locations in the "piston mode" under the petroleum generation expansion force, forming deep basin petroleum reservoirs (Fig. 27c). As petroleum charging continued, tight sandstone reservoirs at the sag and slope were full of petroleum, and when the charging range reached the boundary of tight sandstone reservoirs (the critical porosity threshold 10%), charging forces changed from overpressure to buoyancy, and petroleum accumulated at the high structural location of the Es_3^L in the "displacement mode" (Fig. 27c), forming conventional petroleum reservoirs. Conventional petroleum reservoirs and deep basin petroleum reservoirs overlapped and compounded to form the initial DCHA.
3) **Late Ed sedimentation - early uplift stage: DCHA adjustment controlled jointly by faults and sand bodies under buoyancy with a distal petroleum source**. During the late Ed sedimentation-early uplift period, the Es_4^U and Es_3^L shales entered the condensate and wet gas stage and mature oil and gas stage, respectively, while the Es_3^M shales entered only the low-maturity and mature oil generation stage and petroleum expulsion had not yet started. In the early uplift stage (25–22.7 Ma), petroleum generation and expulsion halted, while the activities of the Wendong No. 3 and Xulou Faults became stronger (Jiang et al., 2015; Shi et al., 2007; Tang and Wang, 2008), cut through gypsum layers and the Es_3^L and Es_3^M shales and became effective pathways for vertical petroleum migration. Therefore, petroleum accumulated in the Es_4^U and Es_3^L in the early stage and then migrated vertically along the pathways. At this time, because the Es_3^U and Es_2 sandstone reservoirs were not tight, petroleum accumulated at the high structural location and in the Es_3^U in the slope location under buoyancy in the "displacement mode". Because few faults developed at the sag and slope locations, most petroleum in the Es_4^U and Es_3^L tight reservoirs was preserved. By this time, the Es_3^M sandstone reservoir at the slope location was not tight yet; thus, the small amount of petroleum that accumulated in Es_3^L at the slope location migrated into Es_3^M along fault pathways under buoyancy in the "displacement mode" (Fig. 27d), forming an adjusted conventional petroleum reservoir.
4) **Late Nm sedimentation – current stage: main formation stage of the DCHA under the petroleum generation expansion force with a proximal petroleum source**. After Nm sedimentation, all faults halted and provided good preservation conditions for petroleum in the Dongpu Depression (Jiang et al., 2015; Shi et al., 2007). During late Nm sedimentation, the strata subsided and shales in the sag and slope locations began to generate petroleum again. By this time, the Es_3^U shales entered the low-maturity to mature oil generation stage and had not started petroleum expulsion, while the Es_3^M, Es_3^L, and Es_4^U shales entered the mature oil and gas, condensate and wet gas, and condensate and wet gas stages, respectively, and began to expel massive amounts of petroleum. Moreover, because the faults were all in closed states, thick gypsum layers developed in the Es_3^L and Es_3^M reservoirs, and the Es_4^U, Es_3^L and Es_3^M reservoirs at the slope and sag locations were tight. Therefore, the petroleum generated from multiple source rocks accumulated at the slope and sag locations in the "piston mode" under the petroleum generation expansion force, forming deep basin petroleum reservoirs with a large area. With a continuous petroleum supply into the future, when the sandstone reservoir at the sag location is full of petroleum, petroleum will continue to accumulate in the sandstone reservoir at the slope location in the "piston mode" under petroleum generation pressurization, gradually promoting the petroleum distribution from the sag to the slope. With further petroleum charging, tight sandstone reservoirs at the slope will be full of petroleum, and when the petroleum charging range reaches the boundary of tight sandstone reservoirs (the critical porosity threshold 10%), charging forces will change from overpressure to buoyancy, and charging modes will change from "piston mode" to "displacement mode" simultaneously; thus, petroleum will accumulate in local areas at the slope location (Fig. 27e-f).

6.6. *Accumulation model*

The formation of DCHA in the Dongpu Depression is a dynamic and continuous accumulation process, controlled by the structural evolution, petroleum generation and expulsion history, reservoir tightness history, fault activity, and gypsum layer development. The accumulation model is as follows.

1) **Superimposed accumulation of conventional petroleum reservoirs in multiple strata at the high structural location**. Petroleum accumulated at the high location comes from laminated shales with TOC values >1% in the Es_4^U in the sag (Zhang et al., 2017; Hu et al., 2022), and the petroleum charging occurred during the late Ed sedimentation to the early uplift stage. When petroleum began to charge, sandstone reservoirs in strata were not tight, petroleum generated in the sag center migrated vertically and transversely along faults and sand bodies under buoyancy and then accumulated in sandstone reservoirs at the high structural location in the Es_2. With sufficient petroleum supply, subsequent petroleum will accumulate in the Es_3^U, Es_3^M, Es_3^L, and Es_4^U reservoirs in sequence at the high location.
2) **Superimposed accumulation of conventional and deep basin petroleum reservoirs in multiple strata at the structural slope location**. Two petroleum charging processes occurred at the slope, including the late Ed sedimentation to early uplift stage and middle-late Nm sedimentation to current stage. At the first stage, the Es_2 and Es_3^U sandstone reservoirs were not tight, and petroleum generated in the sag center migrated vertically and transversely along faults and sand bodies under buoyancy. With a continuous petroleum supply, when the Es_2 and Es_3^U sandstone reservoirs were full of petroleum, petroleum continued to accumulate at the slope location, gradually

promoting petroleum distribution in the Es_2 and Es_3^U sandstone reservoirs forming conventional petroleum reservoirs in multiple strata. At the second stage, the Es_3^L, Es_3^M, and Es_4^U sandstone reservoirs were tight, and petroleum generated by each shale stratum accumulated in the lower areas of the respective tight reservoirs in the "piston mode", forming deep basin petroleum reservoirs at the sag location with large areas. With further petroleum supply, when sandstone reservoirs at the sag are full of petroleum, petroleum will continue to accumulate in sandstone reservoirs at slopes in the "piston mode" under petroleum generation pressurization, gradually promoting petroleum distribution from the sag to the slope and forming deep basin petroleum reservoirs in multiple strata.

3) **Superposition continuous distribution development of deep basin oil and gas reservoirs in multiple intervals near the sag.** The petroleum charging process at the middle-late Nm sedimentation stage occurred at the sag location. By this time, the Es_3^L, Es_3^M, and Es_4^U sandstone reservoirs were tight, and petroleum generated by each shale stratum accumulated in the lower areas of the respective tight reservoirs in the "piston mode", forming deep basin petroleum reservoirs at the sag location with large areas and forming deep basin petroleum reservoirs in multiple strata at the sag location.

7. Implications for petroleum exploration, challenges and perspectives

Our study shows that as the depth of the structural location changes from high to slope to sag, four sequential processes are involved in the dynamic, continuous, progressive hydrocarbon accumulation process: the sequential generation of petroleum phases by source rocks, the sequential porosity and permeability decrease in sandstone reservoirs, the sequential evolution of petroleum charging forces, and the sequential evolution of petroleum charging modes. Conventional and deep basin (tight) petroleum reservoirs that constitute DCHAs have three features, i.e., correlated genesis, continuous petroleum accumulation, and sequential petroleum distribution, which reveal a general law for the sequential accumulation and distribution of conventional and deep basin (tight) petroleum reservoirs. Based on this law, the spatial distribution of conventional and tight petroleum reservoirs can be predicted. There are abundant unconventional hydrocarbon resources in the center of a hydrocarbon reservoir when conventional petroleum resources are found, and conversely, the discovery of unconventional hydrocarbon resources indicates that conventional petroleum may exist in neighboring areas (Zhi et al., 2021; Zou et al., 2014).

The sequential accumulation model of DCHAs differs distinctly from the "petroleum system" theory (Magoon and Dow, 1994). 1) Reservoirs include not only sandstone layers in anticline traps at the accumulation terminal but also hydrocarbon generation strata and migration pathways, and further study should focus on all reservoirs within the range of petroleum supply; 2) internal correlations between conventional and tight petroleum reservoirs suggest that they should be investigated together; and 3) studies should not be limited to the "From Source to Trap" perspective that focuses on predicting favorable accumulation zones in petroleum resource evaluation; instead the entire process of petroleum generation, migration, and accumulation should be investigated and all types of petroleum resources should be evaluated from the new perspective of "source rock – sandstone reservoir coupling and sequential accumulation". Therefore, future exploration of conventional and unconventional hydrocarbon resources should adopt an approach of "synchronous study, synchronous deployment, and synchronous exploration", and a "multi-well platform-type factory production mode" to promote the simultaneous exploitation of conventional and unconventional hydrocarbon resources within different structural locations and strata (Zou et al., 2014), accelerate exploration and development, and realize the maximum economic recovery of petroleum resources in petroliferous basins.

Declaration of Competing Interest

We declare that we do not have any commercial or associative interest that represents a conflict of interest in connection with the work submitted.

Acknowledgments

This study was financially supported by National Natural Science Foundation of China (U19B6003-02; 41872148), CNPC "14th Five-Year Plan" major science and technology projects (2021DJ0101), Young Talents Support Project of Beijing Science and Technology Association (ZX20210075), the 973 projects of State Key Basic Research Program of China (2006CB202300, 2011CB2011), China Postdoctoral Science Foundation (2019M660054), AAPG Foundation Grants-in-Aid Program (15388), and Science Projects of the SINOPEC (P15022).

References

Abbad, M., 2012. Combining the micro grain imager with the effective medium theory for quick assessment of the absolute permeability in carbonates. Soc. Pet. Eng. https://doi.org/10.2118/160863-MS.

Asakawa, T., 1995. Outlook for unconventional natural gas resources. J. Jpn. Assoc. Pet. Tech. 60 (2), 128–135. https://doi.org/10.3720/japt.60.128.

Ayers Jr., W.B., 2002. Coalbed gas systems, resources, and production and a review of contrasting cases from the SanJuan and Powder River basins. AAPG Bull. 86 (11), 1853–1890. https://doi.org/10.1306/61EEDDAA-173E-11D7-8645000102C1865D.

Bao, J., Wu, Y., 2019. Preparation method of cast thin sections. Liaoning Chem. Ind. 48 (06), 531–533. https://doi.org/10.14029/j.cnki.issn1004-0935.2019.06.012.

Berkenpas, P.G., 1991. The Milk River Shallow Gas Pool: role of the updip water trap and connate water in gas production from the pool. Soc. Pet. Eng. https://doi.org/10.2118/22922-MS.

Bourgoyne, A.T., 1990. Shale water as a pressure support mechanism in gas reservoirs having abnormal formation pressure. J. Pet. Sci. Eng. 3 (4), 305–319. https://doi.org/10.1016/0920-4105(90)90051-4.

Brown, C.A., Crafton, I.W., Golson, I.G., 1982. The niobrara gas play: exploration and development of a low-pressure, low-penneability gas reservoir. J. Pet. Technol. 34, 2863–2870. https://doi.org/10.2118/10304-PA.

Cai, J.C., Jin, T.X., Kou, J., et al., 2021. Lucas–Washburn Equation-Based Modeling of capillary-driven flow in porous systems. Langmuir 37 (5), 1623–1636.

Cant, D.J., 1983. Spirit River Formation—A stratigraphic-diagenetic gas trap in the Deep Basin of Alberta. AAPG Bull. 67 (4), 577–587. https://doi.org/10.1306/03B5B65F-16D1-11D7-8645000102C1865D.

Cant, D.J., 1986. Diagenetic traps in sandstones. AAPG Bull. 70, 155–160. https://doi.org/10.1306/9488564C-1704-11D7-8645000102C1865D.

Cao, J., Xia, L., Wang, T., Zhi, D., Tang, Y., Li, W., 2020. An alkaline lake in the late Paleozoic Ice Age (LPIA): a review and new insights into paleoenvironment and petroleum geology. Earth Sci. Rev. 202, 103091.

Chakhmakhchev, A., Suzuki, M., Takayama, K., 1997. Distribution of alkylated dibenzothiophenes in petroleum as a tool for maturity assessments. Org. Geochem. 26 (7), 483–489. https://doi.org/10.1016/S0146-6380(97)00022-3.

Cheng, F., Song, G., Liu, Y., Jin, Q., Sun, F., 2015. Acta Petrol. Sin. 36 (11), 1349–1357. https://doi.org/10.7923/syxb201511004.

Craig, J., Hakhoo, N., Bhat, G.M., Hafiz, M., Khan, M.R., Misra, R., Pandita, S.K., Raina, B.K., Thurow, J., Thusu, B., Ahmed, W., Khullar, S., 2018. Petroleum systems and hydrocarbon potential of the North-West Himalaya of India and Pakistan. Earth Sci. Rev. 187, 109–185. https://doi.org/10.1016/j.earscirev.2018.09.012.

Dmitriy, S., Timothy, K., Jonathan, A., Nico, P., 2011. A multimodal 3D imaging study of natural gas flow in tight sands. Soc. Pet. Eng. https://doi.org/10.2118/146611-MS.

Du, H., Yu, X., Chen, F., 2008. Sedimentary characteristics and petroleum geological significance of salt rock in the third member of Shahejie Formation, Dongpu Sag, Henan Province. J. Paleogeogr. 10 (01), 53–62.

Duan, H., Gao, P., Wang, X., Gao, Y., Ma, C., 2008. Reservoir-forming mechanism and mode of deep oil and gas in north Dongpu Depression. Fault-Block Oil Gas Field 15 (02), 12–15.

EIA, 2019. International Energy Outlook. https://www.eia.gov/outlooks/ieo/.

Etherington, J.R., McDonald, L.R., 2004. Is bitumen a petroleum reserve? Soc. Pet. Eng. https://doi.org/10.2118/90242-MS.

Exxon, M., 2018. Outlook for Energy: A View to 2040. http://corporate.exxonmobil.com/en/energy/energyoutlook/a-view-to-2040.

George, S.C., Ruble, T.E., Dutkiewicz, A., Eadington, P.J., 2002. Reply to comment by Oxtoby on "Assessing the maturity of oil trapped in fluid inclusions using molecular geochemistry data and visually-determined fluorescence colors". Appl. Geochem. 16 (4), 451–473. https://doi.org/10.1016/S0883-2927(00)00051-2.

Gies, R.M., 1984. Case History for a Major Alberta Deep Basin Gas Trap: The Cadomin FormationCase Study of a Deep Basin Gas Field, 38, pp. 115–140. https://doi.org/10.1306/M38441C5.

Goldstein, R.H., 1994. Systematics of Fluid Inclusions in Diagenetic Minerals. SEPM.31. https://doi.org/10.2110/scn.94.31.

Guo, Y., 2013. Study on the Dynamic Mechanism of the Lower Limit of Buoyancy in Tight Sandstone Reservoirs and its Countermeasures. China University of Petroleum, Beijing.
Guo, J., 2014. Near-Source Hydrocarbon Accumulation Mechanism and Distribution Mode of Continuous Tight Sand Gas Reservoir. China University of Petroleum, Beijing.
Guo, Q., Chen, N., Song, H., Wu, X., Xie, H., 2013. Accumulation models and numerical models of tight oil: a case study from Yanchang Formation in Ordos Basin. Lithol. Reserv. 25 (01) https://doi.org/10.3969/j.issn.1673-8926.2013.01.002, 4-10+20.
Guo, Y., Pang, X., Li, Z., Guo, F., Song, L., 2017. The critical buoyancy threshold for tight sandstone gas entrapment: Physical simulation, interpretation, and implications to the Upper Paleozoic Ordos Basin. J. Pet. Sci. Eng. 149, 88–97. https://doi.org/10.1016/j.petrol.2016.10.004.
Hao, F., 2005. Hydrocarbon Generation Kinetics and Hydrocarbon Accumulation Mechanism in Overpressure Basins. China Social Sciences Press, Beijing.
Hu, T., 2019. Genetic Mechanism and Development Model of Continuous Sandstone Hydrocarbon Accumulation in the Shahejie Formation of Dongpu Depression. China University of Petroleum, Beijing (104 pp).
Hu, T., et al., 2018. Oil content evaluation of lacustrine organic-rich shale with strong heterogeneity: a case study of the Middle Permian Lucaogou Formation in Jimusaer Sag, Junggar Basin, NW China. Fuel. 221, 196–205. https://doi.org/10.1016/j.fuel.2018.02.082.
Hu, T., et al., 2021a. Movable oil content evaluation of lacustrine organic-rich shales: Methods and a novel quantitative evaluation model. Earth Sci. Rev. 214, 103545 https://doi.org/10.1016/j.earscirev.2021.103545.
Hu, T., et al., 2021b. Key factors controlling shale oil enrichment in saline lacustrine rift basin: implications from two shale oil wells in Dongpu Depression, Bohai Bay Basin. Pet. Sci. 18 (S1), 687–711. https://doi.org/10.1007/s12182-021-00564-z.
Hu, T., Pang, X.Q., et al., 2022. Identifying the key source rocks in heterogeneous saline lacustrine shales: Paleogene shales in the Dongpu depression, Bohai Bay Basin, eastern China. AAPG Bull. 103 (6), 1325–1356. https://doi.org/10.1306/01202218109.
Hughes, W.B., 1984. Use of thiophenic organosulfur compounds in characterizing crude oils derived from carbonate versus siliciclastic sources. In: Palacas, J.G. (Ed.), Petroleum Geochemistry and Source Rock Potential of Carbonate Rocks. American Association of Petroleum Geologists. https://doi.org/10.1306/St18443C13.
Hunt, J.M., 1990. Generation and migration of petroleum from abnormally pressured fluid compartments. AAPG Bull. 74 (1), 1–12. https://doi.org/10.1306/0C9B21EB-1710-11D7-8645000102C1865D.
Ji, Y., Zhao, C., Liu, M., 1992. Diagenesis models of S_3^3member in Wenliu area of Dongpu depression. J. Univ. Pet. Chin. 16 (01), 8–17.
Ji, Y., Zhao, C., Liu, M., 1995. Diagenesis of clastic docks in Shahejie Formation, Dongpu Depression and its relation to organic matter evolution. Oil Gas J. 16 (02), 148-154+205.
Jia, C., 2017. Breakthrough and significance of unconventional oil and gas to classical petroleum geological theory. Pet. Explor. Dev. 44 (01), 1–10. https://doi.org/10.1016/S1876-3804(17)30002-2.
Jia, C., Zou, C., Li, J., Li, D., Zheng, M., 2012. Assessment criteria, main types, basic features and resource prospects of the tight oil in China. Acta Pet. Sin. 33 (03), 343–350.
Jiang, Y., Cha, M., 2005. Oil and Gas Geology and Exploration. Petroleum Industry Press.
Jiang, Z., Lin, S., Pang, X., 2006. The comparison of two types of tight sand gas reservoir. Pet. Geol. Exp. 28 (03) (210-214+219).
Jiang, Y., Fang, L., Tan, Y., Mu, X., 2015. Differences and main controlling in Dongpu Sag, factors of accumulation periods Bohai Bay Basin. Geol. Rev. 61 (06), 1321–1331.
Jin, Z., Zhang, J., 1999. Deep basin gas reservoir and its exploration strategy. Pet. Explor. Dev. 26 (01) (24-25+3+11-12).
Jin, Z.J., Zhang, J.C., 2003. Two typical types of mechanisms and models for gas accumulations (in Chinese with English abstract). Acta Pet. Sin. 24 (4), 13–16.
Jin, Z., Zhang, J., Pang, X., 1997. Investigation and Preliminary Research Report of Deep Basin Gas Accumulation Principle, Basic Characteristics and Exploration Technology. Basin and Reservoir Research Center, China University of Petroleum, Beijing.
Khalili, A.D., et al., 2012. Permeability upscaling for carbonates from the pore-scale using multi-scale Xray-CT images. Soc. Pet. Eng. https://doi.org/10.2118/152640-MS.
Larue, D.K., Smithard, M., Mercer, M., 2018. Three deep resource plays in the San Joaquin Valley compared with the Bakken Formation. AAPG Bull. 102 (02), 195–243. https://doi.org/10.1306/04241716143.
Law, B.E., Curtis, J.B., 2002a. Introduction to unconventional petroleum systems. AAPG Bull. 86, 1851–1852. https://doi.org/10.1306/61EEDDA0-173E-11D7-8645000102C1865D.
Law, B.E., Curtis, 2002b. Basin-centered gas systems. AAPG Bull. 86 (11), 1891–1919. https://doi.org/10.1306/61EEDDB4-173E-11D7-8645000102C1865D.
Law, B.E., Dickinson, W.W., 1985. Conceptual model for origin of abnormally pressured gas accumulations in low-permeability reservoirs. AAPG Bull. 69 (8), 1295–1304. https://doi.org/10.1306/AD462BD7-16F7-11D7-8645000102C1865D.
Law, B.E., Spencer, C.W., 1993. Gas in Tight Reservoirs - an Emerging Major Source of Energy. United States Geological Survey, Professional Paper, United States.
Leythaeuser, D., Schaefer, R.G., Yükler, A., 1980. Diffusion of light hydrocarbons through near-surface rocks. Nature (London) 284 (5756), 522–525. https://doi.org/10.1038/284522a0.
Li, L., Lin, R., 2005. Study on maturity of crude oil in west slope of Dongpu Depression using aromatic compounds. Acta Sedimentol. Sin. 23 (02), 361–366.
Li, J.R., Yang, Z., Wu, S., et al., 2021. Key issues and development direction of petroleum geology research on source rock strata in China. Adv. Geo-Energy Res. 5 (2), 121–126.
Li, Q., You, X., Jiang, Z., Zhao, X., Zhang, R., 2017. A type of continuous petroleum accumulation system in the Shulu sag, Bohai Bay basin, eastern China. AAPG Bull. 101 (11), 1791–1811. https://doi.org/10.1306/01251715073.
Liang, Z., Wang, J., Yuan, B., 2017a. Pet. Geophys. 15 (02), 9–15.
Liang, Z., Wang, J., Yuan, B., Chang, Z., 2017b. Overpressure feature and its implications on hydrocarbon accumulation of tight gas reservoirs in Qianliyuan depression. Prog. Geophys. 32 (02), 684–688.
Liu, Y., 2015a. A method of determining distribution of continuous hydrocarbon reservoir in faulted basin-a case of the fourth member of Shahejie Formation in Bonan area. Pet. Geol. Rec. Eff. 22 (02), 1–8. https://doi.org/10.13673/j.cnki.cn37-1359/te.2015.02.001.
Liu, Z., 2015b. Steps to China's carbon peak. Nature (London) 522 (7556), 279. https://doi.org/10.1038/522279a.
Liu, K., Eadington, P., 2005. Quantitative fluorescence techniques for detecting residual oils and reconstructing hydrocarbon charge history. Org. Geochem. 36 (7), 1023–1036. https://doi.org/10.1016/j.orggeochem.2005.02.008.
Liu, J., Jiang, Y., 2013. Thermal evolution characteristics of Paleogene source rocks and their main controlling factors in northern part of Dongpu depression. Geol. China 40 (02), 498–507.
Liu, T., Liu, J., 2018. Quantitative evaluation on overpressure generated from undercompaction and fluid expansion. Acta Petrol. Sin. 39 (09), 971–979. https://doi.org/10.7623/syxb201809002.
Liu, K., Eadington, P., Middleton, H., Fenton, S., Cable, T., 2007. Applying quantitative fluorescence techniques to investigate petroleum charge history of sedimentary basins in Australia and Papuan New Guinea. J. Pet. Sci. Eng. 57 (1–2), 139–151. https://doi.org/10.1016/j.petrol.2005.11.019.
Liu, K., et al., 2013. Hydrocarbon charge history of the Tazhong Ordovician reservoirs, Tarim Basin as revealed from an integrated fluid inclusion study. Pet. Explor. Dev. 40 (02), 171–180. https://doi.org/10.1016/S1876-3804(13)60021-X.
Liu, J., Jiang, Y., Tan, Y., Mu, X., 2014a. Relationship between Gypsum-salt rock and oil-gas in Dongpu depression of Bohai Bay Basin. Acta Sedimentol. Sin. 32 (01), 126–137. https://doi.org/10.14027/. cnki cjxb 2014.01015.
Liu, K., et al., 2014b. Innovative fluorescence spectroscopic techniques for rapidly characterising oil inclusions. Org. Geochem. 72, 34–45. https://doi.org/10.1016/j.orggeochem.2014.04.010.
Liu, M., et al., 2014c. Coupling relationship between sandstone reservoir densification and hydrocarbon accumulation: a case from the Yanchang Formation of the Xifeng and Ansai areas, Ordos Basin. Pet. Explor. Dev. 41 (02), 168–175. https://doi.org/10.1016/S1876-3804(14)60021-5.
Liu, K., et al., 2016. Quantitative fluorescence technique of reservoir and its application in hydrocarbon accumulation research. Earth Sci. 41 (03), 373–384.
Loucks, R.G., Reed, R.M., Ruppel, S.C., Jarvie, D.M., 2009. Morphology, genesis, and distribution of nanometer-scale pores in siliceous mudstones of the Mississippian Barnett Shale. J. Sediment. Res. 79 (12), 848–861. https://doi.org/10.2110/jsr.2009.092.
Lu, S., 2008. Oil and Gas Geochemistry. Petroleum Industry Press.
Lu, S., Zhao, X., Wang, Z., Liu, X., Huang, D., 1996. Simulation experiment of coal-derived hydrocarbon generation and migration—characteristics and significance of aromatic products. Acta Petrol. Sin. 17 (1), 47–53.
Lu, X., Jiang, Y., Chang, Z., Wu, X., 2007. Calculation of the erosion thickness of Dongying formation in Dongpu depression and its significance. Geol. Sci. Tech. Inf. 26 (02), 8–12.
Ma, Z., 2008. Dynamic Mechanism and Development Model of Deep Tight Sandstone Reservoirs. China University of Petroleum, Beijing.
Mackenzie, A.S., Brooks, J., Welte, D., 1984. Applications of biological markers in petroleum geochemistry. In: Advances in Petroleum Geochemistry. Academic Press, London, pp. 115–214.
Magoon, L.B., Dow, W.G., 1994. The Petroleum System—From Source to Trap. https://doi.org/10.1306/M60585.
Masters, J.A., 1979. Deep basin gas trap, Western Canada. AAPG Bull. 63, 152–181. https://doi.org/10.1306/C1EA55CB-16C9-11D7-8645000102C1865D.
Masters, J.A., 1984. Lower Cretaceous Oil and Gas in Western Canada. Elmworth - Case Study of a Deep Basin Gas Field, 38, pp. 1–33. https://doi.org/10.1306/M38441C1.
Matthews, K.J., et al., 2016. Global plate boundary evolution and kinematics since the late Paleozoic. Glob. Planet. Chang. 146, 226–250. https://doi.org/10.1016/j.gloplacha.2016.10.002.
Mccollough, E.H., 1934. Structural influence on the accumulation of petroleum in California: Part IV. Relations of petroleum accumulation to structure. AAPG Bull. 735–760. https://doi.org/10.1306/SV6334C34.
Mehmani, A., Tokan-Lawal, A., Prodanovic, M., 2011. The Effect of Microporosity on Transport Properties in Tight Reservoirs, Society of Petroleum Engineers Unconventional Gas Conference. Society of Petroleum Engineers Americas Unconventional Gas Conference, Wondlands, TX(US), pp. 1–14.
Min, L.Y., Lv, C.Y., Zhang, B.W., Li, G.M., Cui, H.Y., 1999. The Porosity and Permeability Measurement of Core in Net Confining Stress (SY/T 6385–1999.). State Bureau of Petroleum and Chemical Industries, Beijing.
Montgomery, S.L., Tabet, D.E., Barker, C.E., 2002. Upper cretaceous Ferron Sandstone: major coalbed methane play in Central Utah. AAPG Bull. 85 (2), 199–219. https://doi.org/10.1306/8626C799-173B-11D7-8645000102C1865D.
Munz, I.A., 2001. Petroleum inclusions in sedimentary basins: systematics, analytical methods and applications. Lithos. 55 (1), 195–212. https://doi.org/10.1016/S0024-4937(00)00045-1.

Osborne, M.J., Swarbrick, R.E., 1997. Mechanisms for generating overpressure in sedimentary basins: a reevaluation: Reply. AAPG Bull. 90 (81), 1023–1041. https://doi.org/10.1306/522B49C9-1727-11D7-8645000102C1865D.
Pang, X., Jin, Z., Zuo, S., 2000. Dynamics, models and classification of hydrocarbon accumulations. Earth Sci. Front. 7, 507–514. China University of Geosciences, Beijing.
Pang, X., Jin, Z., Jiang, Z., Gong, G., Wang, H., 2003. Critical condition for gas accumulation in the deep basin trap and physical modeling. Nat. Gas Geosci. 14 (03), 207–214.
Pang, X., et al., 2012. Dynamic field division of hydrocarbon migration, accumulation and hydrocarbon enrichment rules in sedimentary basins. Acta. Geol. Sin. (Beijing) 86 (6), 1559–1592.
Pang, X., Jiang, Z., Huang, H., Chen, D., Jiang, F., 2014a. Formation mechanisms, distribution models, and prediction of superimposed, continuous hydrocarbon reservoirs. Acta Petrol. Sin. 35 (05), 795–828.
Pang, X., et al., 2014b. Formation, distribution, exploration, and resource/reserve assessment of superimposed continuous gas field in Marsel exploration area, Kazakhstan. Acta Petrol. Sin. 35 (06), 1012–1056.
Pang, X., et al., 2020. A unified model for the formation and distribution of both conventional and unconventional hydrocarbon reservoirs. Geosci. Front. 2, 695–711. https://doi.org/10.1016/j.gsf.2020.06.009.
Pang, X., et al., 2021. Buoyance-driven hydrocarbon accumulation depth and its implication for unconventional resource prediction. Geosci. Front. 12 (4) https://doi.org/10.1016/j.gsf.2020.11.019.
Pang, X., Shao, X., Li, M., Hu, T., Wang, W., 2021a. Correlation and difference between conventional and unconventional reservoirs and their unified genetic classification. Gondwana Res. 97 (6) https://doi.org/10.1016/j.gr.2021.04.011.
Pang, X., Shao, X., Li, M., Hu, T., Wang, W., 2021b. Correlation and difference between conventional and unconventional reservoirs and their unified genetic classification. Gondwana Res. 97 (6), 73–100. https://doi.org/10.1016/j.gr.2021.04.011.
Peng, J., et al., 2017. Geochemistry, origin, and accumulation of petroleum in the Eocene Wenchang Formation reservoirs in Pearl River Mouth Basin, South China Sea: a case study of HZ25-7 oil field. Mar. Pet. Geol. 80, 154–170. https://doi.org/10.1016/j.marpetgeo.2016.08.007.
Peters, K.E., Moldowan, J.M., 1993. The Biomarker Guide: Interpreting Molecular Fossils in Petroleum and Ancient Sediments, United States.
Peters, K.E., Walters, C.C., Moldowan, J.M., 2005. The Biomarker Guide, 2nd. Cambridge University Press, Cambridge.
Ping, H., Chen, H., Thiéry, R., George, S.C., 2017. Effects of oil cracking on fluorescence color, homogenization temperature and trapping pressure reconstruction of oil inclusions from deeply buried reservoirs in the northern Dongying Depression, Bohai Bay Basin, China. Mar. Pet. Geol. 80, 538–562. https://doi.org/10.1016/j.marpetgeo.2016.12.024.
Pollastro, R.M., 2007. Total petroleum system assessment of undiscovered resources in the giant Barnett Shale continuous (unconventional) gas accumulation, Fort Worth Basin, Texas. AAPG Bull. 91 (4), 551–578. https://doi.org/10.1306/06200606007.
Qi, X., Huang, X., Shou, J., Li, Y., 1992. Salt rock, oil and gas in Dongpu Sag. Acta Petrol. Sin. 13 (01) (27-29+23-26).
Radke, M., 1988. Application of aromatic compounds as maturity indicators in source rocks and crude oils. Mar. Pet. Geol. 5 (3), 224–236. https://doi.org/10.1016/0264-8172(88)90003-7.
Radke, M., Welte, H.D., 1983. The Methylphenanthrene Index (MPI) : a Maturity Parameter Based on Aromatic Hydrocarbonsorganic Geochemistry.
Radke, M., Garrigues, P., Willsch, H., 1990. Methylated dicyclic and tricyclic aromatic hydrocarbons in crude oils from the Handil field, Indonesia. Org. Geochem. 15 (1), 17–34. https://doi.org/10.1016/0146-6380(90)90182-Y.
Rahmanian, M.R., Aguilera, R., Kantzas, A., 2011. A new unified diffusion-viscous flow model based on pore level studies of tight gas formations. Soc. Pet. Eng. https://doi.org/10.2118/149223-MS.
Rose, P.R., 1981. Possible basin centered gas accumulation, Roton Basin, Sourthern Colorad. Oil Gas J. 82 (10), 190–197.
Schenk, C.J., 2005. Geologic Definition of Conventional and Continuous Accumulations in Select US Basins – The 2001 Approach, Abstract for AAPG Hedberg Research Conference on Understanding, Exploring and Developing Tight Gas Sands, Vail, Colorado, USA.
Schmoker, J.W., 1995. Method for assessing continuous-type (unconventional) hydrocarbon accumulations. In: Gautier, D.L., Dolton, G.L., Takahashi, K.I., Varnes, K.L. (Eds.), National assessment of United States Oil and Gas Resources—Results, Methodology, and Supporting Data: U.S. Geological Survey Digital Data Series, 30, CD-ROM.
Schmoker, J.W., 2002. Resource-assessment perspectives for unconventional gas systems. AAPG Bull. 86 (11), 1993–1999. https://doi.org/10.1306/61EEDDDC-173E-11D7-8645000102C1865D.
Seifert, W.K., Moldowan, J.M., 1986. Use of biological markers in petroleum exploration. Meth. Geochem. Geophys. 24, 261–290.
Shi, D., Wang, Y., Wang, Y., Yang, G., 2007. Preliminary study on the conditions and characteristics of the Neogene hydrocarbon net blanket accumulation in Dongpu Sag, linqing depression. Chin. J. Geol. 42 (03), 417–429.
Silin, D., Kneafsey, T.J., Ajo-Franklin, J.B., Nico, P., 1984. Gas generation and migration in the Deep Basin of Western Canada. AAPG Mem. 38, 35–47. https://doi.org/10.1306/M38441C2.
Spencer, C.W., 1987. Hydrocarbon generation as a mechanism for overpressuring in Rocky Mountain Region. AAPG Bull. 71 (4), 368–388. https://doi.org/10.1306/94886EB6-1704-11D7-8645000102C1865D.
Spencer, C.W., Mast, R.F., 1986. Geology of tight gas reservoirs, 24. Am. Assoc. Pet. Geol. 24 https://doi.org/10.1306/St24459.
Su, H., et al., 2006. Tectonic evolution and extensional pattern of rifted basin : a case study of Dongpu depression. Oil Gas Geol. 27 (01), 70–77.
Surdam, R.C., Jiao, Z.S., Jie, L., 1995. Pressure regime in the upper cretaceous shales and sandstones in the Washakie Basin, Wyoming. In: Siliciclastic Diagenesis and Fluid Flow: Concepts and Applications, 55, pp. 205–223. https://doi.org/10.2110/pec.96.55.0059.
Surdam, R.C., Jiao, Z.S., Yin, P., 1996. Fluid-flow regimes and sandstone/shale diagenesis in the powder river basin, Wyoming. In: Siliciclastic Diagenesis and Fluid Flow: Concepts and Applications, 55, pp. 59–72. https://doi.org/10.2110/pec.96.55.0059.
Tang, M., Wang, H., 2008. Mar. Geol. Quat. Geol. 28 (03), 55–59.
Tao, S., 2006. Sequence of diagenetic authigenic mineral: the basis of timing the inclusions formation in sedimentary rocks. Pet. Explor. Dev. 33 (02), 154–160.
Tao, S., Zou, C., Wang, J., Fan, J., 2011. On the identification of connotation,extension, and type for some hydrocarbon accumulations. Nat. Gas Geosci. 22 (04), 571–575.
Tissot, B.P., Welte, D.H., 1978. Petroleum Formation and Occurrence : A New Approach to Oil and Gas Exploration.
Tyler, R., Scott, A.R., Kaiser, W.R., Nance, H.S., Mcmurry, R.G., 1995. Geologic and Hydrologic Controls Critical to Coalbed Methane Producibility and Resource Assessment: Williams Fork Formation, Piceance Basin, Northwest Colorado. Topical report, December 1, 1993-November 30, 1995.
Walls, J.D., 1982. Tight gas sands-penneability, pore structure, and clay. J. Pet. Technol. 34 (11), 2708–2714. https://doi.org/10.2118/9871-PA.
Wang, J., 2000. Prospects for large tight sandstone Gas-bearing Regions in China. Nat. Gas Ind. 20 (01), 10–16.
Wang, C., Xia, Y., 1995. Detection and genesis of de-A-ring aromatic triterpenoids in Jurassic lignite from Turpan-Hami Basin. Acta Sedimentol. Sin. 13 (S1), 138–146. https://doi.org/10.14027/j. cnki. cjxb.1995. sl.018.
Wang, M., et al., 2015. Shale oil occurring between salt intervals in the Dongpu Depression, Bohai Bay Basin, China. Int. J. Coal Geol. 152, 100–112. https://doi.org/10.1016/j.coal.2015.07.004.
Wang, R., Tang, Z., Wang, J., Liu, Z., Xia, C., 2018. Prog. Geophys. 33 (03), 1149–1154.
Welte, D., Schaefer, R., Stoessinger, W., et al., 1984. Gas generation and migration in the Deep Basin of Western Canada. AAPG Mem. 38, 35–47. https://doi.org/10.1306/M38441C2.
White, I.C., 1885. The geology of natural gas. Science 5, 521–522. https://doi.org/10.1126/science.ns-5.125.521.
Wilkinson, J.J., Lonergan, L., Fairs, T., Herrington, R.J., 1998. Fluid inclusion constraints on conditions and timing of hydrocarbon migration and quartz cementation in Brent Group reservoir sandstones, Columba Terrace, northern North Sea. J. Avian Biol. 144 (1), 69–89. https://doi.org/10.1144/GSL.SP.1998.144.01.06.
Wilson, W.B., 1934. Proposed classification of oil and gas reservoirs: part IV. Relations of petroleum accumulation to structure. AAPG Bull. 433–445.
Wu, H., Liang, X., Xiang, C., Wang, Y., 2007. Discussion on the characteristics and accumulation mechanism of synclinic oil reservoirs in Songliao Basin. Sci. China Earth Sci. 37 (02), 185–191.
Xu, H., 1991. Characteristics of tight sand gas reservoir in Zhongyuan oil field and its exploration. Acta Petrol. Sin. 12 (01), 1–8.
Yang, Z., Zou, C.N., Gu, Z., et al., 2022. Geological characteristics and main challenges of onshore deep oil and gas development in China. Adv. Geo-Energy Res. 6 (3), 264–266.
Zhang, J., 2001. Prediction of Deep Basin Gas Accumulation and Distribution. China University of Geosciences, Beijing.
Zhang, J., 2003. Research progress of root-edge gas (deep basin gas). Geosci. 17 (02), 210.
Zhang, L., Huang, D., 1997. Compositional characteristics of polycyclic aromatic hydrocarbons in some marine source rocks. Pet. Explor. Dev. 24 (02) (10-15+96-97).
Zhang, J., Jin, Z., Yuan, M., Zhang, J., 2003. Mechanic spectrum for the migration and accumulation of hydrocarbons. Geosci. 17 (03), 323–330.
Zhang, J., Xu, B., Nie, H., Deng, F., 2007. Two essential gas accumulations for natural gas exploration in China. Nat. Gas Ind. 27 (11) (1-6+129).
Zhang, J.C., Xuan, T., Bian, R.K., Bo, X.U., Hui, X., Nie, H.K., et al., 2008. Dynamic equations for nonassociated gas accumulation. Pet. Explor. Dev. 35 (1), 73–79.
Zhang, J., et al., 2015. New progress and reference significance of overseas tight oil exploration and development. Acta Petrol. Sin. 36 (02), 127–137.
Zhang, Z., et al., 2016. Pet. Explor. Dev. 43 (4), 590–599.
Zhang, H., Xu, T., Zhang, Y., 2017. Development characteristics and significance of high quality source rocks of salty lake in Dongpu Depression. Fault-Block Oil Gas Field. 24 (04), 437–441. https://doi.org/10.6056/dkyqt201704001.
Zhang, Y., Luo, H., Wang, C., 2021. Progress and trends of global carbon neutrality pledges. Clim. Chang. Res. 17 (01), 88–97. https://doi.org/10.12006/j.issn.1673-1719.2020.241.
Zhao, J., 2012. Zhao Jingzhou. Conception, classification and resource potential of unconventional hydrocarbons. Nat. Gas Geosci. 23 (03), 393–406.
Zhao, W., et al., 2004. The intension and signification of "Sag-wide Oil- Bearing Theory" in the Hydrocarbon-rich Depression with terrestrial origin. Pet. Explor. Dev. 31 (02), 5–13.
Zhao, J., et al., 2013. Hydrocarbon accumulation patterns of large tight oil and gas fields. Oil Gas Geol. 34 (05), 573–583. https://doi.org/10.11743/ogg20130501.
Zhao, J., et al., 2016. Petroleum accumulation from continuous to discontinuous : concept, classification and distribution. Acta Petrol. Sin. 37 (02), 145–159. https://doi.org/10.7623/syxb201602001.
Zhao, J., Li, J., Xu, Z., 2017. Advances in the origin of overpressures in sedimentary basins. Acta Petrol. Sin. 38 (09), 973–998. https://doi.org/10.7623/syxb201709001.

Zhi, D., et al., 2021. Orderly coexistence and accumulation models of conventional and unconventional hydrocarbons in lower Permian Fengcheng Formation, Mahu sag, Junggar Basin. Pet. Explor. Dev. 48 (01), 38–51. https://doi.org/10.11698/PED.2021.01.04.

Zhu, Z., Jiang, Y., Cheng, Z., 2009. Evaluating maturity of source rocks by aromatic compounds:A case from Dongling Block, Songliao basin. Pet. Explor. Dev. 36 (06), 790–796.

Zou, C., et al., 2009a. The formation conditions and distribution characteristics of continuous petroleum accumulations. Acta Petrol. Sin. 30 (03), 324–331.

Zou, C., et al., 2009b. Global importance of "continuous" petroleum reservoirs: Accumulation, distribution and evaluation. Pet. Explor. Dev. 36 (06), 669–682. https://doi.org/10.1016/S1876-3804(10)60001-8.

Zou, C., et al., 2013. Continuous hydrocarbon accumulation over a large area as a distinguishing characteristic of unconventional petroleum: the Ordos Basin, North-Central China. Earth Sci. Rev. 126, 358–369. https://doi.org/10.1016/j.earscirev.2013.08.006.

Zou, C., et al., 2014. Conventional and unconventional petroleum "orderly accumulation": Concept and practical significance. Pet. Explor. Dev. 41 (1), 14–30. https://doi.org/10.1016/S1876-3804(14)60002-1.

Zou, C., et al., 2015. Formation, distribution, potential and prediction of global conventional and unconventional hydrocarbon resources. Dev. Pet. Explor. Dev. 42 (01), 14–28. https://doi.org/10.1016/S1876-3804(15)60002-7.

Zou, C., et al., 2019. Organic-matter-rich shales of China. Earth Sci. Rev. 189, 51–78. https://doi.org/10.1016/j.earscirev.2018.12.002.

Zuo, Y., et al., 2017. Present temperature field and Cenozoic thermal history in the Dongpu depression, Bohai Bay Basin, North China. Mar. Pet. Geol. 88, 696–711. https://doi.org/10.1016/j.marpetgeo.2017.08.037.